Biol Cybern (2007) 97:63–79
DOI 10.1007/s00422-007-0160-6

ORIGINAL PAPER

Biological Cybernetics

High-frequency oscillations as a consequence of neglected serial damping in Hill-type muscle models

Michael Günther · Syn Schmitt · Veit Wank

Received: 13 November 2006 / Accepted: 28 March 2007 / Published online: 28 June 2007
© Springer-Verlag 2007

Abstract High-frequency vibrations e.g., induced by legs impacting with the ground during terrestrial locomotion can provoke damage within tendons even leading to ruptures. So far, macroscopic Hill-type muscle models do not account for the observed high-frequency damping at low-amplitudes. Therefore, former studies proposed that protective damping might be explained by modelling the contractile machinery of the muscles in more detail, i.e., taking the microscopic processes of the actin–myosin coupling into account. In contrast, this study formulates an alternative hypothesis: low but significant damping of the passive material in series to the contractile machinery—e.g., tendons, aponeuroses, titin—may well suffice to damp these hazardous vibrations. Thereto, we measured the contraction dynamics of a piglet muscle–tendon complex (MTC) in three contraction modes at varying loads and muscle–tendon lengths. We simulated all three respective load situations on a computer: a Hill-type muscle model including a contractile element (CE) and each an elastic element in parallel (PEE) and in series (SEE) to the CE pulled on a loading mass. By comparing the model to the measured output of the MTC, we extracted a consistent set of muscle parameters. We varied the model by introducing either linear damping in parallel or in series to the CE leading to accordant re-formulations of the contraction dynamics of the CE. The comparison of the three cases (no additional damping, parallel damping, serial damping) revealed that serial damping at a physiological magnitude suffices to explain damping of high-frequency vibrations of low amplitudes. The simulation demonstrates that any undamped serial structure within the MTC enforces SEE-load eigenoscillations. Consequently, damping must be spread all over the MTC, i.e., rather has to be de-localised than localised within just the active muscle material. Additionally, due to suppressed eigenoscillations Hill-type muscle models taking into account serial damping are numerically more efficient when used in macroscopic biomechanical neuro-musculo-skeletal models.

M. Günther · S. Schmitt
Eberhard-Karls-Universität,
Institut für Astronomie und Astrophysik,
Abteilung Theoretische Astrophysik, Biomechanik-Gruppe,
Auf der Morgenstelle 10 C,
72076 Tübingen, Germany

M. Günther
Eberhard-Karls-Universität, Orthopädische Klink,
Biomechaniklabor, Hoppe-Seyler-Straße 3,
70276 Tübingen, Germany

M. Günther
Friedrich-Schiller-Universität, Institut für Sportwissenschaft,
Lehrstuhl für Bewegungswissenschaft, Seidelstraße 20,
07749 Jena, Germany

M. Günther (✉) · V. Wank
Eberhard-Karls-Universität, Institut für Sportwissenschaft,
Arbeitsbereich III, Wilhelmstraße 124, 72074 Tübingen, Germany
e-mail: guenther@tat.physik.uni-tuebingen.de

S. Schmitt
Albert-Ludwigs-Universität,
Institut für Sport und Sportwissenschaft,
Schwarzwaldstraße 175, 79117 Freiburg, Germany

List of symbols

MTC	Muscle–tendon complex
CE	Contractile element
PE	Parallel element
PEE	Parallel elastic element
SE	Serial element
SEE	Serial elastic element

SOL	M. soleus
FDS	M. flexor digitorum superficialis
GM	M. gastrocnemius medialis
GL	M. gastrocnemius lateralis
q	normalised muscle activation
q_0	minimum value of q
$\dot{q}$	time derivative of q
τ_q	time constant of rising activation
β_q	ratio between τ_q and time constant of falling activation
STIM	Muscle stimulation
l_{CE}	length of CE
$\dot{l}_{\mathrm{CE}} = v_{\mathrm{CE}}$	contraction velocity of CE
l_0	mean anatomical length of MTC
l_{m}	length of model MTC
$l_{\mathrm{m},0}$	typical length of model MTC
$\dot{l}_{\mathrm{m}}$	velocity of model MTC
F_{m}	force of model MTC
F_{SEE}	force of SEE
F_{PEE}	force of PEE
F_{CE}	force of CE
l_{SE}	length of SE
$l_{\mathrm{SEE},0}$	rest length of SEE
$l_{\mathrm{SEE,nll}}$	length of SEE at non-linear-linear transition in $F_{\mathrm{SEE}}(l_{\mathrm{SE}})$
$\Delta U_{\mathrm{SEE,nll}}$	relative stretch at non-linear-linear transition in $F_{\mathrm{SEE}}(l_{\mathrm{SE}})$
$\Delta F_{\mathrm{SEE},0}$	force at non-linear-linear transition in $F_{\mathrm{SEE}}(l_{\mathrm{SE}})$
$\Delta U_{\mathrm{SEE,l}}$	relative stretch in linear part for force increase $\Delta F_{\mathrm{SEE},0}$
$K_{\mathrm{SEE,l}}$	stiffness of the linear part of $F_{\mathrm{SEE}}(l_{\mathrm{SE}})$
ν_{SEE}	exponent of $F_{\mathrm{SEE}}(l_{\mathrm{SE}})$ in the non-linear part
$K_{\mathrm{SEE,nl}}$	factor of non-linearity in $F_{\mathrm{SEE}}(l_{\mathrm{SE}})$
F_{isom}	normalised isometric force–length relation of CE
$l_{\mathrm{CE,opt}}$	optimal fibre length
$\nu_{\mathrm{CE,limb}}$	exponent of $F_{\mathrm{isom}}(l_{\mathrm{CE}})$ on either ascending or descending limb
ΔW_{limb}	width of $F_{\mathrm{isom}}(l_{\mathrm{CE}})$ on either ascending or descending limb
$F_{\max}$	maximum isometric force
A_{rel}	coordinate of pole in $\dot{l}_{\mathrm{CE}}(F_{\mathrm{CE}})$ normalised to current isometric force $F_{\max}\, q\, F_{\mathrm{isom}}(l_{\mathrm{CE}})$
$A_{\mathrm{rel},0}$	maximum value of A_{rel}
B_{rel}	coordinate of pole in $F_{\mathrm{CE}}(\dot{l}_{CE})$ normalised to $l_{\mathrm{CE,opt}}$
$B_{\mathrm{rel},0}$	maximum value of B_{rel}
$v_{\max}$	concentric contraction velocity at $F_{\mathrm{CE}} = 0$
$v_{\max,0}$	maximum concentric contraction velocity
$L_{A_{\mathrm{rel}}}$	length dependency of A_{rel}
$L_{B_{\mathrm{rel}}}$	length dependency of B_{rel}
$Q_{A_{\mathrm{rel}}}$	activation dependency of A_{rel}
$Q_{B_{\mathrm{rel}}}$	activation dependency of B_{rel}
$l_{\mathrm{PEE},0}$	rest length of PEE
ν_{PEE}	exponent of $F_{\mathrm{PEE}}(l_{CE})$
K_{PEE}	factor of non-linearity in $F_{\mathrm{PEE}}(l_{\mathrm{CE}})$
$\mathcal{F}_{\mathrm{PEE}}$	force of PEE if l_{CE} is stretched to $\Delta W_{\mathrm{limb=des}}$
$\mathcal{L}_{\mathrm{PEE},0}$	rest length of PEE normalised to $l_{\mathrm{CE,opt}}$
F_{EPS}	numerical limit for defining zero $F_{\mathrm{isom}}(l_{\mathrm{CE}})$
$dVdF_{\mathrm{con}}$	inclination of linear concentric continuation of $\dot{l}_{\mathrm{CE}}(F_{\mathrm{CE}})$ for $F_{\mathrm{CE}} < 0$
S_{ecc}	step in inclination of $F_{\mathrm{CE}}(\dot{l}_{\mathrm{CE}} = 0)$ between eccentric and concentric force–velocity relation(s)
$\mathcal{F}_{\mathrm{ecc}}$	coordinate of pole in $\dot{l}_{\mathrm{CE}}(F_{\mathrm{CE}})$ normalised to $F_{\max}\, q\, F_{\mathrm{isom}}(l_{\mathrm{CE}})$ for $\dot{l}_{\mathrm{CE}} > 0$
F_{trans}	force where linear continuation of eccentric $\dot{l}_{\mathrm{CE}}(F_{\mathrm{CE}})$ relation starts
v_{trans}	velocity where linear continuation of eccentric $\dot{l}_{\mathrm{CE}}(F_{\mathrm{CE}})$ relation starts
$dVdF_{\mathrm{ecc}}$	inclination of linear eccentric continuation of $\dot{l}_{\mathrm{CE}}(F_{\mathrm{CE}})$ for $F_{\mathrm{CE}} > F_{\mathrm{trans}}$
l_{PE}	length of PEE ($= l_{\mathrm{CE}}$)
d_{PE}	(constant) damping coefficient of PE
d_{SE}	damping coefficient of SE
$d_{\mathrm{SE,max}}$	maximum value in $d_{\mathrm{SE}}(l_{\mathrm{CE}}, q)$
R_{SE}	minimum value of d_{SE} normalised to $d_{\mathrm{SE,max}}$
D_{SE}	dimensionless factor to scale $d_{\mathrm{SE,max}}$
$\dot{l}_{\mathrm{SE}} = v_{\mathrm{SE}}$	contraction velocity of SE
t	time
$\mathbf{g}$	vector of gravitational acceleration
d_{ext}	modelled external damping

1 Introduction

It is known that stress, strain, strain rate, frequency, and number of cycles exceeding tolerances of biological materials may cause damage (Biewener 1990; Ker and Zioupos 1997; Ker et al. 2000; Alexander 2001; Zioupos et al. 2001;

Currey 2002). Nature has developed structures and strategies to face potentially hazardous implications. Specifically, in muscle–tendon structures high-frequency oscillations have been identified to cause fatigue failure of tendons (Ker and Zioupos 1997). Here, damping within the activated muscle tissue has been proposed as a suitable protection strategy (Wilson et al. 2001).

In analogy to Wilson et al. (2001) and Siebert et al. (2003), we observed oscillations of the loading mass when trying to simulate concentric muscle contraction experiments with an established Hill-type muscle model (Zajac 1989; van Leeuwen 1992; van Soest and Bobbert 1993; Meijer et al. 1998; Ettema and Meijer 2000; Günther and Ruder 2003). It is also known that Hill-type muscle models fail to describe energy absorption of high-frequency oscillations at low amplitudes. Wilson et al. (2001) concluded that a more detailed muscle model based on a microscopic description of sarcomere dynamics (Piazzesi and Lombardi 1995, 1996) would be appropriate to explain energy absorption within the activated muscle tissue. However, they did not verify whether the low but significant damping within the passive tendinous tissue (Ker 1981; Riemersma and Schamhardt 1985; Shadwick 1990; Alexander 2001) might be sufficient for high-frequency damping.

Consequently, in this study we checked for damping within passive collagenous tissue to provide a valid alternative mechanism for high-frequency energy absorption. Thereto, first we measured the output of an isolated piglet muscle–tendon complex (MTC) within three contraction modes at various loading masses and MTC-lengths. Second, we mathematically formulated the contraction dynamics of a muscle model including a Hill-type contractile element (CE), a parallel elastic (PEE) and a serial elastic (SEE) element, and dampers added either in parallel or in series to the CE. Third, we extracted the parameters of the muscle model including serial damping by fitting the simulation results to the experimental data of all loading situations. Finally, a comparison of the experimental data to the simulation results with and without parallel or serial damping verifies the physiological significance of both damping mechanisms.

2 Methods

The following methods section first contains the description of the experimental data acquisition and second the simulation part with a detailed muscle model formulation.

2.1 Experiment

2.1.1 Subjects and instrumentation

The experimental results presented and used for model evaluation in this paper are from investigations of the calf muscle group of one normal weight one day old piglet (body weight: 1,510 g). The animal belongs to the crossbreed of Piétrain × German Landrace. Measurement data were obtained from isometric, concentric and quick-release contractions under different conditions. These experiments were part of studies focused on comparison of skeletal muscle performance in normal weight and intrauterine growth retarded newborn piglets. The committee of the Thuringian state government for animal research approved the protocol of the study. The animals were managed in accordance with the guidelines of the European Community and the American Physiological Society. The protocol for animal preparation and physiological monitoring during the measurement of muscle performance is fully described in Wank et al. (2000). Therefore, at this point the presentation of the experimental setup focuses on methods of stimulation and muscle contraction measurement and on the experimental protocol.

For analysis of stimulated muscle contractions of the piglet plantar flexors the piglet was taken in prone position (Fig. 1). The tibia bone was carefully fixed on proximal and distal ends by steel mandrills and the hip was fixed by a horizontal iron rod so that the femur and consequently the origins of the stimulated muscles were kept unchanged (Fig. 2). The forces for plantar flexion in pigs are generated mainly by four muscles with different specific weight and fibre type composition at birth: soleus (SOL), flexor digitorum superficialis (FDS), medial and lateral gastrocnemius (GM, GL) (Wank et al. 2006). The anatomical muscle parameters are listed in Table 1.

Under isometric conditions the muscle force was transferred to a force transducer via a calcaneus clamp and a steel wire (Fig. 1, top). The lower leg of the animal and the transducer were aligned in such a way that the longitudinal axis of the calf muscles and the wire to the transducer ran horizontally. The force signal of a strain gauge transducer (type 11E-100N0, Sensotec, USA; ± 100 N, 0.5 µm/N compliance) was amplified by a DC-amplifier (ME-10, Hottinger–Baldwin, Germany). After A/D conversion the data was sampled with 1, 000 Hz and stored on a PC.

For analysis of concentric contractions the steel wire from the calcaneus was diverted by a reel of 100 mm circumstance to a load stamp ($m = 100$ g) that was hanging in the gravitation field (Fig. 1, bottom). The shortening of the muscle was transmitted by the reel to the axis of an encoder (Jenoptik, Jena, 20000 impulses per round). In this way, the shortening of contraction of the calf muscles could be measured with a resolution of 5 µm. Digital impulses from the encoder were counted and sampled with 1,000 Hz via PC. From raw data the contraction velocity and the muscle force was computed by derivation. Thereto, recorded time curves of muscle length were smoothed using spline functions (Reinsch 1967). The load of contraction could be changed by fixing iron discs of different mass on the load

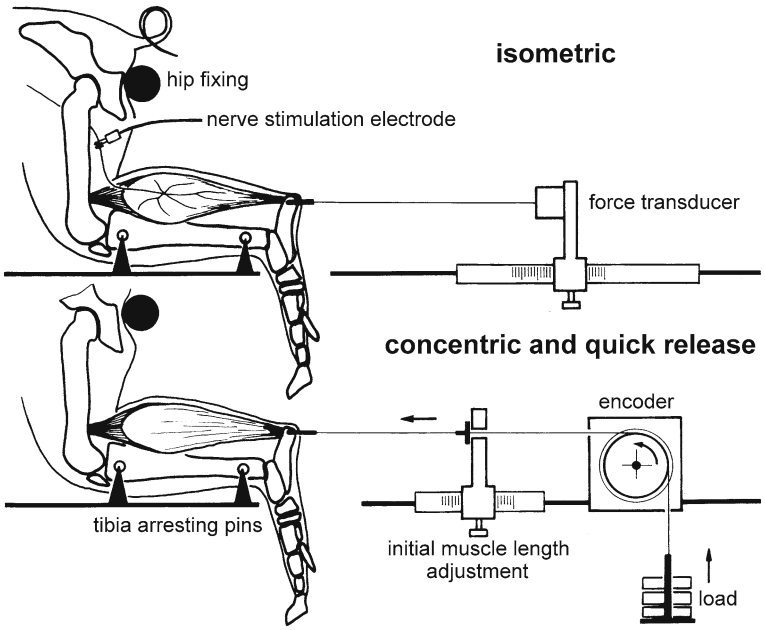

Fig. 1 The setup of plantar flexor muscle contraction (*top* isometric, *bottom* concentric and quick-release) experiments for a piglet. The skeleton is carefully fixed in prone position keeping the origins of the stimulated muscles unchanged. This allowed to measure the net output of the four main contributing muscle–tendon complexes (MTCs) depicted in Fig. 2

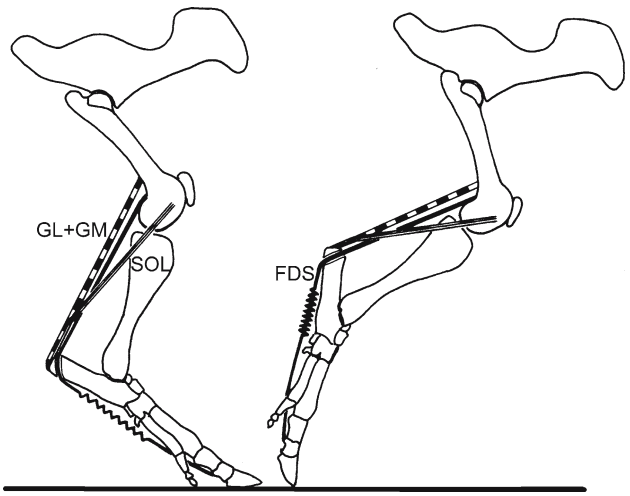

Fig. 2 Anatomical muscle structure of a piglet. Depicted muscles are M. gastrocnemius medialis (*GM*), M. gastrocnemius lateralis (*GL*), M. soleus (*SOL*) and M. flexor digitorum superficialis (*FDS*). The net output of these four MTCs is measured (Fig. 1). Their anatomical parameters are listed in Table 1. The parameters of the lumped model MTC (Fig. 3) reflecting the experimental situation are given in Table 2

stamp. To avoid different initial length of the muscle because of varying loads, the initial length was fixed at resting muscle length with a 100 g load. For this a clamp was adjusted on the steel wire against a fixed bar. For analysis of quick-release contractions according to Hill (1938) the load stamp could be fixed using an electromagnet. In this mode of analysis the load stamp was held in fixed position until 1.0 s after electrically stimulating the muscle. Thus, it was ensured that the isometric force of the plantar flexors had risen to the maximum value. Thereafter, the load stamp was released. Data recording (encoder) and processing was analogous to concentric contractions described above.

For calf muscle stimulation the sciatic nerve of the left hind limb was used. For this purpose a skin incision was made in the lateral upper leg. The sciatic nerve was carefully prepared and attached to a platinum electrode pair immersed by Ringer solution in order to avoid desiccating the nerve. Bipolar stimulation of the sciatic nerve was used for supramaximal muscle contraction (voltage-constant rectangular pulses, 150 Hz repetition frequency, 100 µs impulse width; Physiostimulator, Hugo Sachs Elektronik, Germany). During the experiments stimulation nerve and electrodes were superfused with warmed physiological saline (37°C). In order to avoid an influence of force output measured on the calcaneus by ankle torque due to a simultaneous contraction of the muscle antagonists the distal tendons of tibialis anterior and extensor digitorum longus were sectioned. After the surgical preparation had been completed general anesthesia was changed by exchange of isoflurane inhalation against intravenous thiobarbital infusion (12.5 mg/(kg[body weight]h)). Furthermore, an epidural blockade was done after lumbar puncture below the fourth lumbar vertebra by instillation of 0.5–1.0 ml of the local anesthetic bupivacaine hydrochloride (Fa. Curasan, Germany). Exact setting of the transmission blockade was verified by an immediate tonus loss of the hind limb muscles. Then, the piglet was allowed to rest for approximately 30 min until the beginning of the measurement series of different muscle contractions.

2.1.2 Experimental protocol

First, a series of isometric force measurements at different muscle length with 2 s stimulation and 2 min resting period (adjusting the next muscle length) was carried out. Based on

Table 1 Mean anatomical muscle parameters (compare Fig. 2) from five ($n = 5$) normal weight 1 day old piglets (mean body weight $\approx$ 1,500 g; see (Wank et al. 2000) for estimated muscle mass, pennation angle, and fibre type I; see (Wank 2000) for length of muscle belly, aponeurosis length, fibre geometry, pennation angle, fibre length, and tendon length; see (Wank et al. 2006) for estimated muscle mass and fibre type II)

	GL	GM	SOL	FDS
Estimated muscle mass (g)	2.0	2.5	1.0	1.0
Length of muscle belly (m)	0.044 ± 0.004	0.04 ± 0.004	0.044 ± 0.004	0.045 ± 0.005
Aponeurosis length (m)	0.033 ± 0.003	0.028 ± 0.003	0.006 ± 0.001	0.039 ± 0.004
Fibre geometry	Unipennate	Unipennate	Fusiform	Bipennate
Pennation angle (°)	18 ± 4	15 ± 4	4 ± 1	13 ± 3
Fibre length (m)	0.012 ± 0.003	0.013 ± 0.003	0.039 ± 0.004	0.008 ± 0.002
Tendon length (m)	0.015 ± 0.002	0.018 ± 0.003	0.014 ± 0.003	0.056 ± 0.006
Fibre type I (slow twitch) (%)	8.2 ± 5.9	8.5 ± 4.6	5.3 ± 3.2	25.0 ± 5.4
Fibre type II (fast twitch) (%)	91.8 ± 5.9	91.5 ± 4.6	94.7 ± 3.2	75.0 ± 5.4

these data the mean anatomical length of the muscle–tendon complex (MTC) l_0 of the plantar flexors was estimated. l_0 is of significance for the validation of the muscle model (see beginning of Sects. 3.1, 3.1.4 and 4.1). Thereafter, a series of (initially unloaded) concentric contractions was analysed. At first, the initial muscle length was adjusted corresponding to muscle strain at 100 g load. Contractions with loads of 100, 200, 300, 400, 600, 800, 1,000, 1,400 and 1,800 g were recorded twice for each load (1 s stimulation duration, 2 min resting period). In the same way quick-release contractions were investigated—as well twice for each load and 2 min rest after each trial. In contrast to concentric mode the stimulation duration at quick-release mode was 1.5 s (1 s isometric pre-contraction and 0.5 s after release). For checking fatigue effects at the end of each series an isometric contraction at the mean anatomical muscle length l_0 was recorded again after concentric and quick-release series. The maximum isometric force of the reference trials were generally above 95% of the initial value from the first series.

2.2 Simulation

For the simulation study we mapped the experimental setup (Sect. 2.1) to a mechanical model, including one lumped muscle–tendon complex (MTC) fixed to the inertial system pulling on the centre of mass of a rigid body (Fig. 3). The loading masses ranged from 100 to 1,800 g. The whole model was implemented in a simulation package *simsys* developed in our department (Krieg 1992; Günther and Ruder 2003) based on the Shampine and Gordon (1975) integration algorithm and a linear equation solver from *Numerical Recipes* (Press et al. 1994). We simulated the three experimental situations with the identical code by switching one input

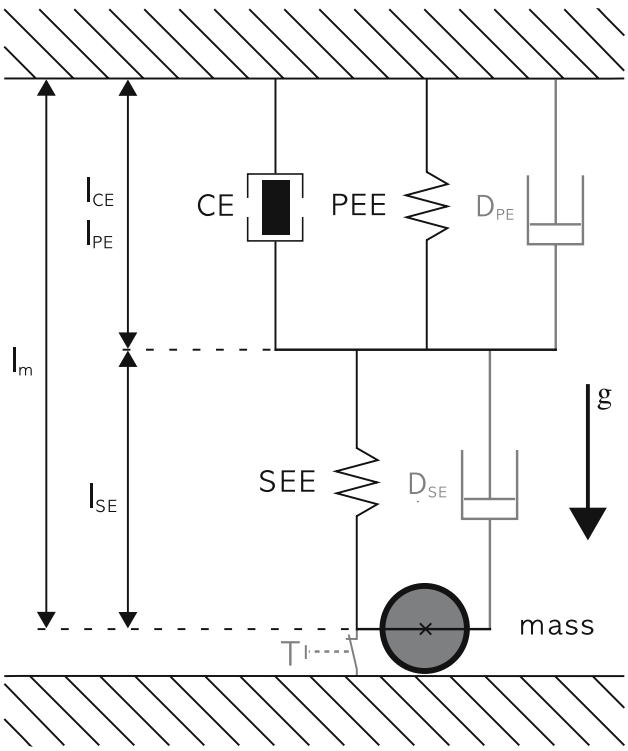

Fig. 3 The structure of the lumped model MTC (actual length: l_m). l_m is the sum of the length of the contractile element (CE) l_{CE} plus the length of the serial element (SE; serial elastic element: SEE) l_{SE}. The length of the parallel element (PE; parallel elastic element: PEE) equals l_{CE}. The standard Hill-type muscle model is drawn with *solid black lines*. Optionally added damping components (D_{PE} and D_{SE}) are greyed out. The experimental procedure for the three different contraction modes differs in switching the trigger T (isometric: T locked; concentric: T released; quick-release: T release after full activation). The MTC-length l_m was varied during isometric contractions, the loading mass during concentric and quick-release contractions. **g** means the gravitational acceleration vector

Table 2 Parameters of a lumped model MTC (GL, GM, SOL, FDS; compare Figs. 1, 2, 3) for a 1 day old piglet (body weight: 1,510 g) used in all simulations

Activation dynamics (Zajac)	$\tau_q\,(s)$ $\frac{1}{40}$	β_q 1.0	q_0 0.0001			
Isometric force	$F_{\max}\,(\mathrm{N})$ 30.0	$l_{\mathrm{CE,opt}}\,(m)$ 0.015	ΔW_{des} 0.14	$v_{\mathrm{CE,des}}$ 3.0	ΔW_{asc} 0.57	$v_{\mathrm{CE,asc}}$ 4.0
Contraction dynamics (concentric: Hill)[a]	$A_{\mathrm{rel},0}$ 0.1	$B_{\mathrm{rel},0}\,(\frac{1}{\mathrm{s}})$ 1.0				
Contraction dynamics (eccentric: van Soest)	S_{ecc} 2.0	$\mathcal{F}_{\mathrm{ecc}}$ 1.8				
Parallel elastic element[b]	$\mathcal{L}_{\mathrm{PEE},0}$ 0.9	v_{PEE} 2.5	$\mathcal{F}_{\mathrm{PEE}}$ 1.0			
Serial elastic element[c]	$l_{\mathrm{SEE},0}\,(\mathrm{m})$ 0.045	$\Delta U_{\mathrm{SEE,nll}}$ 0.1825	$\Delta U_{\mathrm{SEE},l}$ 0.073	$\Delta F_{\mathrm{SEE},0}\,(\mathrm{N})$ 60.0		
Damping parameters	$d_{\mathrm{PE}}\,(\mathrm{Ns/m})$ 6.0	$d_{\mathrm{SE}}\,(\mathrm{Ns/m})$ 6.0	D_{SE} 0.3	R_{SE} 0.01		

Dependent parameters:
[a] $v_{\max,0} = \frac{B_{\mathrm{rel},0}}{A_{\mathrm{rel},0}}\, l_{\mathrm{CE,opt}} = 0.15\,\mathrm{m/s}$
[b] $K_{\mathrm{PEE,nl}} = 3.86 \times 10^7\,\mathrm{N/m}^{2.5}$
[c] $v_{\mathrm{SEE}} = 2.5,\ K_{\mathrm{SEE,nl}} = 9.82 \times 10^6\,\mathrm{N/m}^{2.5},\ K_{\mathrm{SEE},l}(30\,\mathrm{N}) = 1.20 \times 10^4\,\mathrm{N/m},\ \Delta U_{\mathrm{SEE}}(30\,\mathrm{N}) = 0.138$

parameter. All muscle parameters used in our simulations are summarised in Table 2.

2.2.1 Starting point

In our muscle model both the activation dynamics and the contraction dynamics of a muscle are described by each a first order differential equation. According to Hatze (1977, 1981) and Zajac (1989) the muscle activation q represents the Ca^{2+}-concentration (biochemical state) of the muscle caused by neural stimulation STIM (q and STIM defined relative to their physiological maxima). Therefore, q scales the current isometric force. The term "stimulation" (van Soest and Bobbert 1993; Günther and Ruder 2003; Kistemaker et al. 2006) is applied in equivalence to the term "excitation" as used by Zajac (1989) who promoted to model neural input signals by just one parameter instead of two (Hatze 1977, 1981).

Specifically, we modified the activation dynamics described by Zajac (1989) with respect to a non-zero minimum value q_0 (Hatze 1977, 1981) for the activation $q_0 \leq q \leq 1$ (Günther and Ruder 2003):

$$\dot{q} = \frac{1}{\tau_q}\left(\mathrm{STIM} - \mathrm{STIM}\,(1-\beta_q)\,(q-q_0) - \beta_q\,(q-q_0)\right). \quad (1)$$

Hereby, τ_q means the time constant for rising activation, β_q the ratio between τ_q and the time constant for falling activation (Zajac 1989), and $0 \leq \mathrm{STIM} \leq 1$ the current stimulation of the contractile element (CE). Hatze (1977) formulated a more complex function $\dot{q} = \dot{q}(l_{\mathrm{CE}}, q)$ (l_{CE}: length of the contractile element, see Fig. 3), which was used by van Soest and Bobbert (1993) in jumping simulations. Our starting point for modelling the contraction dynamics was formulated by van Soest and Bobbert (1993)

$$\dot{l}_{\mathrm{CE}} = \dot{l}_{\mathrm{CE}}(l_{\mathrm{m}}, l_{\mathrm{CE}}, q) \quad (2)$$

who derived it from the empirical relation $F_{\mathrm{m}} = F_{\mathrm{m}}(\dot{l}_{\mathrm{m}})$ ["Hill equation", Hill (1938)]. Here, l_{m} means the length of the model MTC (index m) and F_{m} its force. In the following F will generally be used as force symbol. The internal structure of the muscle model is depicted in Fig. 3. The contraction dynamics (Eq. 2) then directly follows from interpreting the "Hill equation" as the dynamic characteristic of the contractile element force development by solving the force equilibrium

$$F_{\mathrm{SEE}}(l_{\mathrm{m}}, l_{\mathrm{CE}}) = F_{\mathrm{PEE}}(l_{\mathrm{CE}}) + F_{\mathrm{CE}}(l_{\mathrm{CE}}, \dot{l}_{\mathrm{CE}}, q) \quad (3)$$

for the contraction velocity $\dot{l}_{\mathrm{CE}}$ of the contractile element. Thereby, SEE represents the serial elastic element and PEE the parallel elastic element.

2.2.2 Exchanged model functions

Based on the aforementioned starting point (van Soest and Bobbert 1993), we replaced three features within the contraction dynamics of muscle model by more detailed functional dependencies. First of all, refining the approach of a non-linear SEE-characteristic (van Soest and Bobbert 1993), we allowed the SEE for a continuously differentiable transition between an initial non-linear region and a constant stiffness at higher loads (Fig. 4). This is due to the fact that data from

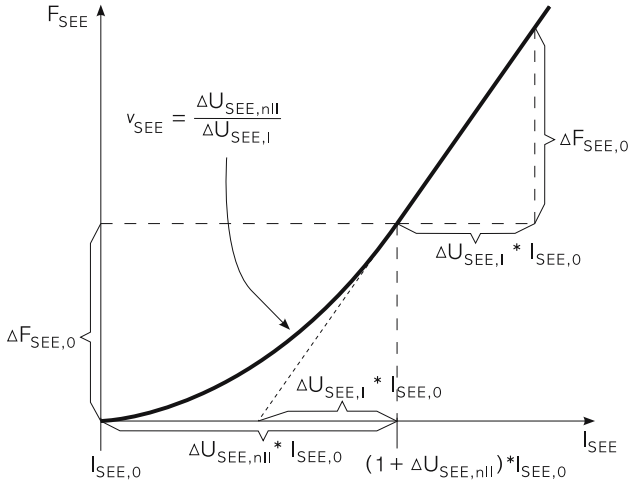

Fig. 4 The force–length relation of the SEE. Four independent parameters are used: $l_{\mathrm{SEE},0}$ (rest length), $\Delta U_{\mathrm{SEE,nll}}$ (relative stretch at non-linear-linear transition), $\Delta F_{\mathrm{SEE},0}$ (both force at the transition and force increase in the linear part), and $\Delta U_{\mathrm{SEE},l}$ (relative additional stretch in the linear part providing a force increase of $\Delta F_{\mathrm{SEE},0}$). The transition between the initial non-linear and the linear region is located at $l_{\mathrm{SEE,nll}} = (1+\Delta U_{\mathrm{SEE,nll}})\, l_{\mathrm{SEE},0}$, the exponent for the initial non-linear relation is $\nu_{\mathrm{SEE,nll}} = \Delta U_{\mathrm{SEE,nll}}/\Delta U_{\mathrm{SEE,l}}$. The parameters are given in Table 2

literature are ambigous (Proske and Morgan 1987; van Ingen Schenau 1984) as to whether tendon material shows such a transition. Therefore, the force F_{SEE} acting in the serial elastic element (SEE) writes

$$F_{\mathrm{SEE}}(l_{\mathrm{SE}}) = \begin{cases} 0, & l_{\mathrm{SE}} < l_{\mathrm{SEE},0} \\ K_{\mathrm{SEE,nl}}\,(l_{\mathrm{SE}} - l_{\mathrm{SEE},0})^{\nu_{\mathrm{SEE}}}, & l_{\mathrm{SE}} < l_{\mathrm{SEE,nll}} \\ \Delta F_{\mathrm{SEE},0} + K_{\mathrm{SEE},l}\,(l_{\mathrm{SE}} - l_{\mathrm{SEE,nll}}), & l_{\mathrm{SE}} \geq l_{\mathrm{SEE,nll}} \end{cases} \tag{4}$$

where $l_{\mathrm{SE}} = l_{\mathrm{m}} - l_{\mathrm{CE}}$ is the length of the serial element (SE) and

$$l_{\mathrm{SEE,nll}} = (1+\Delta U_{\mathrm{SEE,nll}})\, l_{\mathrm{SEE},0}$$

$$\nu_{\mathrm{SEE}} = \Delta U_{\mathrm{SEE,nll}}/\Delta U_{\mathrm{SEE},l}$$

$$K_{\mathrm{SEE},nl} = \Delta F_{\mathrm{SEE},0}/(\Delta U_{\mathrm{SEE,nll}}\, l_{\mathrm{SEE},0})^{\nu_{\mathrm{SEE}}}$$

$$K_{\mathrm{SEE},l} = \Delta F_{\mathrm{SEE},0}/(\Delta U_{\mathrm{SEE},l}\, l_{\mathrm{SEE},0})$$

represent the parameters introduced in Eq. 4, which in turn are derived from the input parameters $l_{\mathrm{SEE},0}$ (rest length), $\Delta U_{\mathrm{SEE,nll}}$ (relative stretch at non-linear-linear transition), $\Delta F_{\mathrm{SEE},0}$ (both force at the transition and force increase in the linear part), and $\Delta U_{\mathrm{SEE},l}$ (relative additional stretch in the linear part providing a force increase of $\Delta F_{\mathrm{SEE},0}$).

Second, the length dependency of the isometric force

$$F_{\mathrm{isom}}(l_{\mathrm{CE}}) = \exp\left\{ \left| \frac{l_{\mathrm{CE}}/l_{\mathrm{CE,opt}} - 1}{\Delta W_{\mathrm{limb}}} \right|^{\nu_{\mathrm{CE,limb}}} \right\} \tag{5}$$

e.g., also suggested by Hatze (1977, 1981) replaced a parabolic characteristic. Here, $l_{\mathrm{CE,opt}}$ is the optimal fibre length, ΔW_{limb} means the width of the normalised bell curve in the respective limb (ascending or descending: Fig. 5) and $\nu_{\mathrm{CE,limb}}$ its exponent (Hatze 1981: ν_{CE}=2).

Third, we took into account that experimental findings show that the Hill parameters determining the contraction dynamics (Eq. 2) in fact do depend on length l_{CE} and activation q. Thus, Eq. 2 writes explicitly

$$\dot{l}_{\mathrm{CE}} = B_{\mathrm{rel}}(l_{\mathrm{CE}}, q)\, l_{\mathrm{CE,opt}} \left(1 - \frac{q\, F_{\mathrm{isom}}(l_{\mathrm{CE}}) + A_{\mathrm{rel}}(l_{\mathrm{CE}}, q)}{\frac{F_{\mathrm{CE}}}{F_{\max}} + A_{\mathrm{rel}}(l_{\mathrm{CE}}, q)} \right) \tag{6}$$

setting up $A_{\mathrm{rel}}(l_{\mathrm{CE}}, q) = A_{\mathrm{rel},0}\, L_{A_{\mathrm{rel}}}(l_{\mathrm{CE}})\, Q_{A_{\mathrm{rel}}}(q)$ and $B_{\mathrm{rel}}(l_{\mathrm{CE}}, q) = B_{\mathrm{rel},0}\, L_{B_{\mathrm{rel}}}(l_{\mathrm{CE}})\, Q_{B_{\mathrm{rel}}}(q)$ as product functions. Following (Gordon et al. 1966; Julian 1971; Stern 1974; van Soest and Bobbert 1993) the length dependency of the maximum contraction velocity (at zero load)

$$\begin{aligned} v_{\max}(l_{\mathrm{CE}}, q) &= -\dot{l}_{\mathrm{CE}}(F_{\mathrm{CE}} = 0) \\ &= \frac{B_{\mathrm{rel}}(l_{\mathrm{CE}}, q)}{A_{\mathrm{rel}}(l_{\mathrm{CE}}, q)} l_{\mathrm{CE,opt}}\, q\, F_{\mathrm{isom}}(l_{\mathrm{CE}}) \end{aligned} \tag{7}$$

is assumed as

$$L_{A_{\mathrm{rel}}}(l_{\mathrm{CE}}) = \begin{cases} 1, & l_{\mathrm{CE}} < l_{\mathrm{CE,opt}} \\ F_{\mathrm{isom}}(l_{\mathrm{CE}}), & l_{\mathrm{CE}} \geq l_{\mathrm{CE,opt}} \end{cases} \tag{8}$$

$$L_{B_{\mathrm{rel}}}(l_{\mathrm{CE}}) = 1. \tag{9}$$

Re-interpreting the experimental data from Petrofsky and Phillips (1981) and Chow and Darling (1999), we replaced the dependency of the Hill "constants" on the activation q used by van Soest and Bobbert (1993)

$$Q_{A_{\mathrm{rel}}}(q) = q \tag{10}$$

$$Q_{B_{\mathrm{rel}}}(q) = \begin{cases} q/0.3, & q < 0.3 \\ 1, & q \geq 0.3 \end{cases} \tag{11}$$

by

$$Q_{A_{\mathrm{rel}}}(q) = \frac{1}{4}(1+3\,q) \tag{12}$$

$$Q_{B_{\mathrm{rel}}}(q) = \frac{1}{7}(3+4\,q). \tag{13}$$

As a minor fourth modification, we allowed the characteristic of the parallel elastic element (PEE) for a variable exponent ν_{PEE}

$$F_{\mathrm{PEE}}(l_{\mathrm{CE}}) = \begin{cases} 0, & l_{\mathrm{CE}} < l_{\mathrm{PEE},0} \\ K_{\mathrm{PEE}}\,(l_{\mathrm{CE}} - l_{\mathrm{PEE},0})^{\nu_{\mathrm{PEE}}}, & l_{\mathrm{CE}} \geq l_{\mathrm{PEE},0} \end{cases} \tag{14}$$

with $K_{\mathrm{PEE}} = \mathcal{F}_{\mathrm{PEE}} \frac{F_{\max}}{(l_{\mathrm{CE,opt}}\,(\Delta W_{\mathrm{limb=des}} + 1 - \mathcal{L}_{\mathrm{PEE},0}))^{\nu_{\mathrm{PEE}}}}$ and $l_{\mathrm{PEE},0} = \mathcal{L}_{\mathrm{PEE},0}\, l_{\mathrm{CE,opt}}$ with the three free parameters $\mathcal{F}_{\mathrm{PEE}}$, $\mathcal{L}_{\mathrm{PEE},0}$ and ν_{PEE} (Table 2).

2.2.3 Numerical refinement

The numerical implementation of the first order muscle model (no muscle masses) requires to ascertain the functionality of the numerical algorithms on the limits of validity of the model functions. First, although our function $F_{\mathrm{isom}}(l_{\mathrm{CE}})$ is well defined between $-\infty$ and $+\infty$, we have to make sure that its value does not fall below a numerical limit F_{EPS} as the floating point operation $F_{\mathrm{isom}}/F_{\mathrm{isom}}$ occurs during the computer calculations of e.g., $v_{\max}(l_{\mathrm{CE}}, q)$ in Eq. 7. Still, during simulations the muscle model can be forced into heavy over-stretching and strong shortening situations. In the case $l_{\mathrm{CE}} < 0.01\, l_{\mathrm{CE,opt}}$ we set $\dot{l}_{\mathrm{CE}} = 0$. For $l_{\mathrm{CE}} > 1.99\, l_{\mathrm{CE,opt}}$, we determined the contraction velocity from the first time derivative of the force equilibrium $F_{\mathrm{SEE}}(l_{\mathrm{m}}, l_{\mathrm{CE}}) = F_{\mathrm{PEE}}(l_{\mathrm{CE}})$ (and applying the chain rule) resulting in

$$\dot{l}_{\mathrm{CE}} = \frac{\dot{l}_{\mathrm{m}}}{1 + \left(\frac{\partial F_{\mathrm{PEE}}(l_{\mathrm{CE}})}{\partial l_{\mathrm{CE}}} / \frac{\partial F_{\mathrm{SEE}}(l_{\mathrm{SE}})}{\partial l_{\mathrm{SE}}} \right)}. \tag{15}$$

Additionally, we describe two numerical refinements we implemented. On the one hand, there are two situations during simulations where the equilibrium (Eq. 3) might demand negative contractile element forces F_{CE}. One situation is a malformed initial choice of l_{CE} and the second is caused by $\dot{l}_{\mathrm{m}} < -v_{\max}$ during concentric contraction scenarios enforced by second order external dynamics (loading masses). In these cases we set $\dot{l}_{\mathrm{CE}} = dVdF_{\mathrm{con}} \cdot F_{\mathrm{CE}}$ with $dVdF_{\mathrm{con}} = 10^3\, F_{\max}\, l_{\mathrm{CE,opt}}\, B_{\mathrm{rel},0}/A_{\mathrm{rel},0}$, providing high negative contraction velocities at low negative forces. However, during our simulations including the muscle damping mechanisms as described below $\dot{l}_{\mathrm{m}} < -v_{\max}$ was not observed.

On the other hand, an inherent part of the starting point model consists of the continuation of the contraction dynamics into the eccentric region (discontinuity of the derivative at $F_{\mathrm{CE}} = 0$ (Katz 1939): $(\partial F_{\mathrm{CE}}/\partial \dot{l}_{\mathrm{CE}})|_{\dot{l}_{\mathrm{CE}} \to 0_+} = S_{\mathrm{ecc}} \cdot (\partial F_{\mathrm{CE}}/\partial \dot{l}_{\mathrm{CE}})|_{\dot{l}_{\mathrm{CE}} \to 0_-}$) by means of a separate hyperbolic function (van Soest and Bobbert 1993) showing a singularity at $F_{\mathrm{CE}} = \mathcal{F}_{\mathrm{ecc}}\, F_{\max}\, q\, F_{\mathrm{isom}}$. $\mathcal{F}_{\mathrm{ecc}}$ is a multiple of the isometric force $F_{\max}\, q\, F_{\mathrm{isom}}$ (see Table 2). To assure steady integration in the vicinity of the singularity in our implementation of the van Soest and Bobbert (1993) model the eccentric characteristic is extrapolated by a linear function $\dot{l}_{\mathrm{CE}} = dVdF_{\mathrm{ecc}} \cdot (F_{\mathrm{CE}} - F_{\mathrm{trans}}) + v_{\mathrm{trans}}$ with $dVdF_{\mathrm{ecc}} = 10^4\, F_{\max}\, l_{\mathrm{CE,opt}}\, B_{\mathrm{rel},0}/A_{\mathrm{rel},0}$. The parameters F_{trans} and v_{trans} are the coordinates of the continuously differentiable transition between eccentric hyperbola and linear continuation. For two reasons the singularity was only significant in the calculations with the starting point model. These were necessary for comparison to the contraction dynamics including PE- or SE-damping. First, we determined the muscle parameters only on the experimental basis of concentric contractions. Second, even if external dynamics enforced eccentric contractions our concentric solution branches (Sects. 2.2.4,2.2.5, 2.2.6) provided continuous extrapolation into the eccentric region as one can already expect from Eq. 6 without PE- or SE-damping (up to the pole $\dot{l}_{\mathrm{CE}} = B_{\mathrm{rel}}\, l_{\mathrm{CE,opt}}$).

2.2.4 Constant parallel (PE)-damping

Some authors suggest the presence of significant damping in parallel to both PEE and CE (Hatze 1981; Davy and Audu 1987; Schmalz 1993b,a). When adding a damped parallel element (PE: $l_{\mathrm{PE}} = l_{\mathrm{CE}}$) the force equilibrium (Eq. 3) writes

$$\begin{aligned} F_{\mathrm{SEE}}(l_{\mathrm{m}}, l_{\mathrm{CE}}) = {} & F_{\mathrm{PEE}}(l_{\mathrm{CE}}) + d_{\mathrm{PE}}\, \dot{l}_{\mathrm{CE}} \\ & + F_{\mathrm{CE}}(l_{\mathrm{CE}}, \dot{l}_{\mathrm{CE}}, q). \end{aligned} \tag{16}$$

If we now solve Eq. 6 for the contractile force

$$F_{\mathrm{CE}} = F_{\max} \left(\frac{q\, F_{\mathrm{isom}}(l_{\mathrm{CE}}) + A_{\mathrm{rel}}(l_{\mathrm{CE}}, q)}{1 - \frac{\dot{l}_{\mathrm{CE}}}{B_{\mathrm{rel}}(l_{\mathrm{CE}}, q) l_{\mathrm{CE,opt}}}} - A_{\mathrm{rel}}(l_{\mathrm{CE}}, q) \right) \tag{17}$$

and substitute Eq. 17 into Eq. 16 we end up with a quadratic equation for $\dot{l}_{\mathrm{CE}}$:

$$0 = C_2\, \dot{l}_{\mathrm{CE}}^2 + C_1\, \dot{l}_{\mathrm{CE}} + C_0 \tag{18}$$

with the coefficients

$$\begin{aligned} C_2 &= d_{\mathrm{PE}} \\ C_1 &= -(d_{\mathrm{PE}}\, l_{\mathrm{CE,opt}}\, B_{\mathrm{rel}}(l_{\mathrm{CE}}, q) + F_{\mathrm{SEE}}(l_{\mathrm{m}}, l_{\mathrm{CE}}) \\ &\quad - F_{\mathrm{PEE}}(l_{\mathrm{CE}}) + F_{\max}\, A_{\mathrm{rel}}(l_{\mathrm{CE}}, q)) \\ C_0 &= l_{\mathrm{CE,opt}}\, B_{\mathrm{rel}}(l_{\mathrm{CE}}, q)\, (F_{\mathrm{SEE}}(l_{\mathrm{m}}, l_{\mathrm{CE}}) \\ &\quad - F_{\mathrm{PEE}}(l_{\mathrm{CE}}) - F_{\max}\, q\, F_{\mathrm{isom}}(l_{\mathrm{CE}})). \end{aligned} \tag{19}$$

As C_1 and C_0 are always negative the only solution of Eq. 18 providing concentric ($\dot{l}_{\mathrm{CE}} \le 0$) contraction dynamics is

$$\dot{l}_{\mathrm{CE}} = \frac{-C_1 - \sqrt{C_1^2 - 4\, C_2\, C_0}}{2\, C_2}. \tag{20}$$

2.2.5 Constant serial (SE)-damping

Damping coefficients as e.g., d_{PE} are usually extracted from experiments measuring whole muscle visco-elastic properties. However, as these experiments usually examine complex muscle preparations one could also conclude that damping properties might be located in series to the CE (Krause et al. 1995). Thus, for estimating the influence of SE-damping we alternatively introduced a constant SE-damping coefficient d_{SE} instead of a constant PE-damping coefficient d_{PE}. Thus, Eq. 3 becomes

$$F_{\mathrm{SEE}}(l_{\mathrm{m}}, l_{\mathrm{CE}}) + d_{\mathrm{SE}}(\dot{l}_{\mathrm{m}} - \dot{l}_{\mathrm{CE}}) = F_{\mathrm{PEE}}(l_{\mathrm{CE}}) + F_{\mathrm{CE}}(l_{\mathrm{CE}}, \dot{l}_{\mathrm{CE}}, q). \quad (21)$$

Following the same transformational steps as in Sect. 2.2.4, we get again a quadratic equation (Eq. 18) for $\dot{l}_{\mathrm{CE}}$ with the coefficients now writing

$$\begin{aligned} C_2 &= d_{\mathrm{SE}} \\ C_1 &= -(d_{\mathrm{SE}}\,(\dot{l}_{\mathrm{m}} + l_{\mathrm{CE,opt}}\,B_{\mathrm{rel}}(l_{\mathrm{CE}}, q)) \\ &\quad + F_{\mathrm{SEE}}(l_{\mathrm{m}}, l_{\mathrm{CE}}) - F_{\mathrm{PEE}}(l_{\mathrm{CE}}) + F_{\mathrm{max}}\,A_{\mathrm{rel}}(l_{\mathrm{CE}}, q)) \\ C_0 &= l_{\mathrm{CE,opt}}\,B_{\mathrm{rel}}(l_{\mathrm{CE}}, q)\,(d_{\mathrm{SE}}\,\dot{l}_{\mathrm{m}} + F_{\mathrm{SEE}}(l_{\mathrm{m}}, l_{\mathrm{CE}}) \\ &\quad - F_{\mathrm{PEE}}(l_{\mathrm{CE}}) - F_{\mathrm{max}}\,q\,F_{\mathrm{isom}}). \end{aligned} \quad (22)$$

In contrast to Eq. 19 now the solution coefficients in Eq. 22 depend on the known contraction velocity of the MTC $\dot{l}_{\mathrm{m}}$. We found that stable concentric contractions were only possible using the same solution branch (negative sign) as in Eq. 20.

2.2.6 Force-dependent serial (SE)-damping

By using the constant SE-damping coefficient from Sect. 2.2.5 for a range of loading masses, we found that a SE-damping coefficient depending on the loading situation further improves the model validity. Therefore, as a third damping mechanism, we implemented a force-dependent SE-damping. Hence, Eq. 3 becomes

$$\begin{aligned} &F_{\mathrm{SEE}}(l_{\mathrm{m}}, l_{\mathrm{CE}}) + d_{\mathrm{SE,max}}(l_{\mathrm{CE}}, q) \\ &\quad \times \left((1 - R_{\mathrm{SE}})\,\frac{F_{\mathrm{CE}}(l_{\mathrm{CE}}, \dot{l}_{\mathrm{CE}}, q)}{F_{\mathrm{max}}} + R_{\mathrm{SE}}\right)(\dot{l}_{\mathrm{m}} - \dot{l}_{\mathrm{CE}}) \\ &= F_{\mathrm{PEE}}(l_{\mathrm{CE}}) + F_{\mathrm{CE}}(l_{\mathrm{CE}}, \dot{l}_{\mathrm{CE}}, q) \end{aligned} \quad (23)$$

with $d_{\mathrm{SE,max}}(l_{\mathrm{CE}}, q) = D_{\mathrm{SE}}\,\frac{F_{\mathrm{max}}\,A_{\mathrm{rel},0}}{l_{\mathrm{CE,opt}}\,B_{\mathrm{rel},0}}$ (i.e., here a constant as the simplest case) where $0 \leq D_{\mathrm{SE}}, R_{\mathrm{SE}} \leq 1$ are dimensionless constant parameters. In case $R_{\mathrm{SE}} = 1$ the force-dependency vanishes and we get constant SE-damping. Again a quadratic equation in $\dot{l}_{\mathrm{CE}}$ has to be solved and the coefficients emerge as

$$\begin{aligned} C_2 &= d_{\mathrm{SE,max}}(l_{\mathrm{CE}}, q)\,(R_{\mathrm{SE}} - A_{\mathrm{rel}}\,(1 - R_{\mathrm{SE}})) \\ C_1 &= -(C_2\,\dot{l}_{\mathrm{m}} + D_0 + F_{\mathrm{SEE}}(l_{\mathrm{m}}, l_{\mathrm{CE}}) - F_{\mathrm{PEE}}(l_{\mathrm{CE}}) \\ &\quad + F_{\mathrm{max}}\,A_{\mathrm{rel}}(l_{\mathrm{CE}}, q)) \\ C_0 &= D_0\,\dot{l}_{\mathrm{m}} + l_{\mathrm{CE,opt}}\,B_{\mathrm{rel}}(l_{\mathrm{CE}}, q) \\ &\quad \times (F_{\mathrm{SEE}}(l_m, l_{\mathrm{CE}}) - F_{\mathrm{PEE}}(l_{\mathrm{CE}}) - F_{\mathrm{max}}\,q\,F_{\mathrm{isom}}(l_{\mathrm{CE}})) \end{aligned} \quad (24)$$

introducing $D_0 = l_{\mathrm{CE,opt}}\,B_{\mathrm{rel}}(l_{\mathrm{CE}}, q)\,d_{\mathrm{SE,max}}(l_{\mathrm{CE}}, q)(R_{\mathrm{SE}} + (1 - R_{\mathrm{SE}})\,q\,F_{\mathrm{isom}}(l_{\mathrm{CE}}))$ as an abbreviation.

3 Results

Applying the simulation method (Sect. 2.2), we obtained the muscle parameters by fitting the simulation results to an array of 23 muscle output relations (force–time, force–velocity, velocity–time). Hereby, we had to vary approximately 20 parameters and the 23 initial conditions to match the respective measured relations in parallel. We solved this problem by trial and error.

First, we equated the length parameter $l_{\mathrm{CE,opt}}$ with the fibre length (Table 1) knowing that the pennation angles were less than 20° (Zajac 1989). Then, we set $l_{\mathrm{SEE},0}$ to the difference between the anatomical length of the MTC (≈ 0.06 m) and $l_{\mathrm{CE,opt}}$. The maximum isometric force F_{max} was estimated from isometric contractions. These parameters represent the basic physiology of the four main muscles of the hind limb analysed in the experiment described in Sect. 2.1.

The identification of all other parameters (listed in Table 2) is described in the following Sect. 3.1. Based on the resulting validated muscle model, in Sect. 3.2, we derive consequences for muscle modelling and predict internal properties of the muscle.

3.1 Choice of the muscle parameters: model validity

In this section we present the comparison of the simulation with the experiment. Thereby, we follow the main steps during the process of the parameter identification for the three contraction modes of the contractile element. In the experiment the typical initial MTC-length for quick-release and concentric contractions is where the passive muscle shows approximately 1/30 of maximum isometric force resistance. Empirically, the MTC also shows maximum isometric force output around this typical initial MTC-length (therefore named mean anatomical MTC-length l_0, here ≈ 0.06 m), i.e., in the model at about $l_{\mathrm{SEE},0} + l_{\mathrm{CE,opt}}$. To be as consistent as possible with both the mean anatomical MTC-length l_0 and the experimental results of all three contraction modes, we finally used $l_{\mathrm{m},0} = 0.0615\,\mathrm{m} \approx l_0$ as typical MTC-length in the model.

3.1.1 Quick-release experiment

In the quick-release contraction mode the MTC contraction is clearly dominated by the stiffness of the SEE in the vicinity of the operation point of maximum isometric force F_{max}. Presuming realistic starting values of the Hill parameters (e.g., $A_{\mathrm{rel},0} = 0.2$, $B_{\mathrm{rel},0} = 2.0\,\frac{1}{s}$) from literature we get a stiffness $K_{\mathrm{SEE},l}(F_{\mathrm{SEE}} \approx F_{\mathrm{max}}) = 12\,\mathrm{kN/m}$ (Table 2). Figure 5 shows the force–velocity relation of contractions under different loads. The experimental (crossed lines) and the simulation (solid lines) results are plotted for comparison as will be done also for the concentric and isometric contraction mode later.

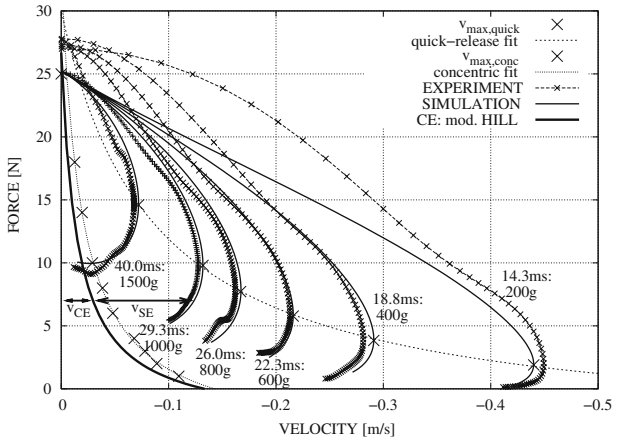

Fig. 5 Quick-release contraction mode. The MTC contracts along the load-dependent force–velocity relation starting (release) at zero velocity. Depicted are the following: (i) the measured force–velocity relations of the MTC (*crossed lines*) for different loads (in g; additionally, the time passed since release in ms), (ii) the associated simulation results (*thin solid lines*), (iii) the concentric force–velocity relation of the model CE for $q = 1$ and $l_{CE} = \frac{2}{3}\, l_{CE,opt}$ (*thick solid line*), (iv) two *arrows* representing the portions of contraction velocity of the CE (v_{CE}) and the SE (v_{SE}) in one exemplary contraction situation (1,000 g load $\approx$ 20 ms after release where the MTC produces $\approx$ 7 N output at a contraction velocity of $\approx 0.12\,\mathrm{m/s}$), and the results of the following two parameter fits. Hill parameters fitted to the points of maximum measured contraction velocities (*upper dotted line through big crosses*) are $F_{max} = 30.0\,\mathrm{N}$, $A_{rel} = 0.125$, $B_{rel} = 5.75\,\frac{1}{s}$ (i.e., $v_{max} = 0.690\,\mathrm{m/s}$). For comparison the maximum velocities of the MTC during concentric contractions (see Fig. 6) are plotted (*lower dotted line through big crosses*) and the respective fitted Hill parameters are $F_{max} = 32.9\,\mathrm{N}$, $A_{rel} = 0.131$, $B_{rel} = 1.25\,\frac{1}{s}$ (i.e., $v_{max} = 0.143\,\mathrm{m/s}$). Note that all simulations (release at $l_{m,0} \approx l_0$ with a fully activated CE at $l_{CE} \approx \frac{2}{3}\, l_{CE,opt}$: compare Fig. 8) start from $\approx$ 25 N force level according to the measured 1,000 g relation (almost perfect concurrence of simulation and experiment). For a possible explanation of non-systematic phenomena in the initial experimental curves see Sect. 3.1.1

Additionally, in Fig. 5 the experimental curves are plotted somehow beyond the maximum velocity, the respective time passed since release is indicated, and the simulation results are drawn accordingly. The percentage of the SE-contraction in the MTC contraction velocity can be directly seen in Fig. 5. Choosing a force level (both arrows: $\approx$ 7 N), we find that the respective current SE-velocity (v_{SE}) is given by the difference between the depicted MTC-velocity and the CE-velocity (v_{CE}) plotted for the initial state of the quick-release contraction (thick solid line, $q = 1, l_{CE} \approx \frac{2}{3}\, l_{CE,opt}$). The determined stiffness is little sensitive to the variability of the Hill parameters known from literature. In contrast, the concentric contraction is far more sensitive to $A_{rel,0}$ and $B_{rel,0}$ than to SEE-stiffness. These parameters are, therefore, obtained from fitting concentric contraction simulations to experimental data as presented in the next paragraph. Few iteration steps are necessary to fit both quick-release and concentric contractions to identify a consistent set of $A_{rel,0}$, $B_{rel,0}$ and $K_{SEE,l}$ ($F_{SEE} \approx F_{max}$). Our model contains no representation of potential history effects within the passive structures (PE, SE) at $t = t_{start}$ in the experimental setup, which may have been absent for the muscle preparation of the 1,000 g contraction. Therefore, we chose the initial muscle length $l_m = 0.0603$ m to be in accordance with the 1,000 g preparation assuming there the least influence of such a preparation effect and consequently showing best concurrence of simulation and experiment.

3.1.2 Concentric contraction

Figure 6 depicts the velocity–time relation of concentric contractions with different loading masses for exactly the same MTC as analysed in the quick-release contraction mode in the preceding Sect. 3.1.1. As criteria for parameter adjustment, we used the amplitude and the timing of the maxima and the frequency of the superimposed oscillation. Initial conditions were $l_m \approx 0.97\, l_{m,0} = 0.0597$ m and $l_{CE} \approx 0.93\, l_{CE,opt} = 0.0140$ m. The load starts to move when the muscle force exceeds gravity which happens in the simulation at an activation level of $q \approx 0.5$ for 100 g and $q \approx 0.99$ for 1,800 g. We observe maximum MTC-velocity amplitudes e.g., for the lowest analysed load (100 g) of 0.11 m/s which is about 25% lower than the maximum CE velocity $v_{max,0}$ (Table 2). Within the displayed time interval of 160 ms internally the CE shortens to $l_{CE} \approx 1/3\, l_{CE,opt}$ (100 g: $\Delta l_{CE} = 0.0087$ m) and $l_{CE} \approx 2/3\, l_{CE,opt}$ (1,800 g: $\Delta l_{CE} = 0.0041$ m). In contrast, externally the MTC shortens ten times more for 100 g ($\Delta l_m = 0.0082$ m) than for 1,800 g ($\Delta l_m = 0.0008$ m). The CE contraction kinematics must closely map the real muscle

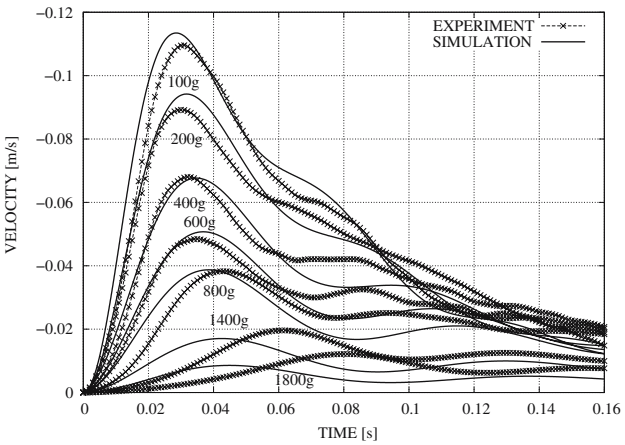

Fig. 6 Concentric contraction mode. The contraction velocity of the MTC in the experiment (*crossed lines*) and associated simulation (*solid lines*) is plotted versus time for various loads (in g). All curves are shifted to the time where the load leaves its support (0.0 s), i.e., when muscle force exceeds gravity. In that instant, despite being fully stimulated ($STIM = 1$, according to the experimental situation) the CE is not fully activated for 100 g ($q \approx 0.54$), however, it is for 1,800 g ($q > 0.999$)

fibre kinematics given a realistic SEE-stiffness in the model and knowing that both model MTC kinematics matches the real MTC kinematics and model MTC-length equals real MTC-length.

Figure 6 also demonstrates that superimposed damped oscillations depending on the load occur in both the experiment and the simulation. They become more accentuated if SE-damping is neglected (compare Sect. 3.2.3 below). The associated frequencies range from 19.0 Hz (100 g) to 10.9 Hz (1,800 g) and are well predicted by the simulation. The mean force level during contraction corresponds to the external load and determines via the non-linearity of the SEE-characteristic the respective force-dependent stiffness of the MTC. Both our analysis of isometric contractions (see next Sect. 3.1.3) and literature account for such a non-linearity. Here, the SEE-stiffnesses range from 1.5 kN/m (100 g) to 9 kN/m (1,800 g). The measured and predicted frequencies of the observed oscillations comply very well with the eigenfrequencies of a linear spring-mass system composed of the loading mass and an SEE-spring linearised around the operation point of the typical load (100 g:19.5 Hz, 1,800 g:11.2 Hz). We conclude that the observed eigenoscillation is that of a loading mass versus the connection point between SEE and CE serving as a virtual suspension point of the spring(SEE)-mass(load) system.

In general, the experimental plots show load-dependent latencies for reaching the maximum contraction velocity which are significantly lower in our model. Additionally, a non-systematic variability of these latencies is manifest in the experimental data. Both these findings and too low velocities in the model at greater shortening of the CE ($t > 100$ ms) are in accordance with the indications from the quick-release contraction mode (potential history effects) suggestive of the lack of an internal dissipative degree of freedom within the muscle model. History characteristics of a real muscle might explain a dependency of the measured data on the preparation process.

3.1.3 Isometric contraction

Having found a basic estimate of the stiffness of the SEE the isometric contraction mode constitutes the basis for finding the parameters of the PEE and substantiates the non-linear characteristic of the SEE. The (passive) muscle forces in the de-activated muscle for different MTC-lengths are transparent in Fig. 7 before stimulation at $t = 1.0$ s. This MTC force–length relation is determined by the SEE and PEE composed in series and shows an exponent of non-linearity of $\approx 2.3 \ldots 2.7$. To reduce complexity and in assumption of comparable material properties, we chose a non-linear exponent of $\nu_{\mathrm{SEE,PEE}} = 2.5$ for both elastic elements. Furthermore, the quick-release experiments govern the linear

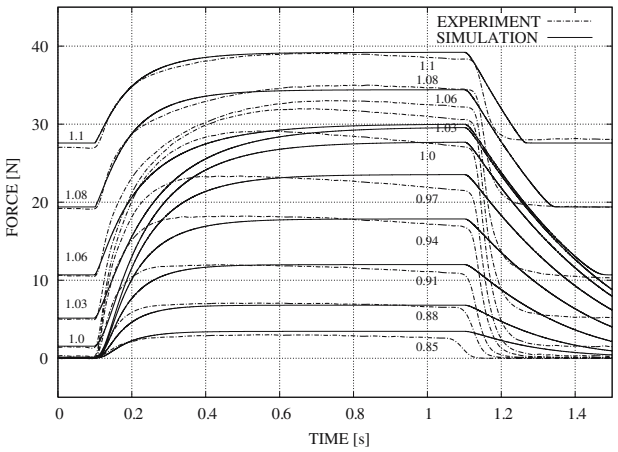

Fig. 7 Isometric contraction mode. Force output of the MTC is plotted versus time for various fixed MTC-lengths (ratios $l_{\mathrm{m}}/l_0 = l_{\mathrm{m}}/l_{\mathrm{m},0}$ are given): experimental curves as *dash-dotted* and simulation as *solid lines*. Full stimulation of the previously passive muscle starts at 0.1 *s* (simulation: $STIM = 1$), it ends at about 1.1 *s*

stiffness of the SEE around the operating point of maximum isometric force. From this, the choice of the non-linear coefficient of the SEE characteristic is restricted. Keeping strictly to the experimental elongation steps, it is possible to find a ratio between the characteristic coefficients of SEE and PEE in the model by reproducing the passive MTC force–length relation. A fine-tuning of this relationship could be achieved by a slight variation of the SEE–PEE coefficient ratio and the rest length of the PEE (parameter: $\mathcal{L}_{\mathrm{PEE},0}$). Additional information for the $\mathcal{L}_{\mathrm{PEE},0}$ choice first came from the fact that the MTC already shows a low but significant passive resistive force at $0.97 l_0$ (0.3 N, not resolved in Fig. 7). Second, there are indications from literature (Granzier and Labeit 2006) that there are elastic structures located within the sarcomere taking over passive forces already slightly below the force–length plateau region. The best choice of the ratio of the non-linear coefficients of the SEE–PEE compound was $K_{\mathrm{PEE,nl}} \approx 4K_{\mathrm{SEE,nl}}$ with $\mathcal{L}_{\mathrm{PEE},0} = 0.90$. Consistently, the mentioned pre-attunement of the SEE-stiffness $K_{\mathrm{SEE,nl}}$ results in simulated concentric contraction dynamics close to the experimental findings (Sect. 3.1.2 above), presuming realistic starting values of the Hill constants from literature. Having specified the elastic parameters of SEE and PEE, the maximum force levels of the fully stimulated muscle at varied fixed lengths determine the four parameters ΔW_{limb}, $\nu_{\mathrm{CE,limb}}$ of both the ascending and descending limb of the isometric force–length relation of our contractile element (CE).

3.1.4 Muscle length and length dependency of the isometric force

Based on the fact that model MTC-length is equal to real MTC-length (within few millimeters) we extract the preset

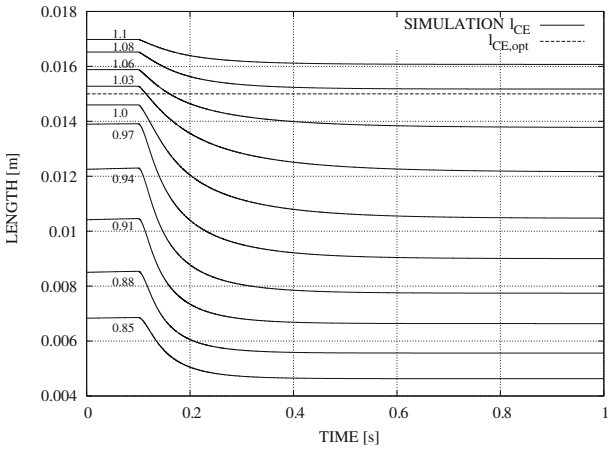

Fig. 8 CE-length during isometric contractions. The CE-lengths from simulations in Fig. 7 ($STIM = 0$, $q = q_0$ before 0.1 s, $STIM = 1$ afterwards) are plotted versus time (*solid lines*) with the fixed ratio $l_m/l_{m,0}$. The optimal CE-length $l_{CE,opt}$ is shown for comparison

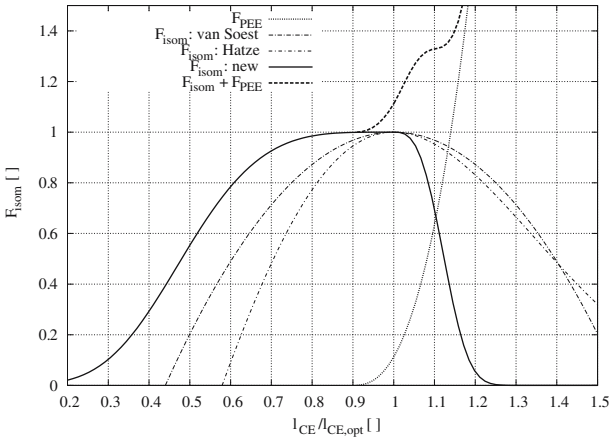

Fig. 9 The normalised isometric force–length relation of the CE. The abscissa is the CE-length l_{CE} normalised to the optimal CE-length $l_{CE,opt}$. The *solid black line* depicts the active maximum ($q = 1$) isometric force (normalised to F_{max}) $F_{isom}(l_{CE})$ of the CE. The *dotted line* represents the respectively normalised passive force–length curve of the PEE. At a given l_{CE} $F_{isom}(l_{CE})\, q\, F_{max} + F_{PEE}(l_{CE})$ (plus optionally the damping force of the PE) is equal to the force in the SE. The *thick dashed line* represents the respective normalised isometric force–length relation of the fully activated CE ($q = 1$). For CE-lengths higher than $l_{CE,opt}$ the PEE increasingly takes over the load from the CE. According to our analysis the CE is not elongated to lengths higher than approximately $l_{CE} = 1.1\, l_{CE,opt}$ in the steady state during isometric contractions (compare Fig. 8 at $l_m = 1.1\, l_{m,0}$). For comparison two alternative modelled force–length relations of the CE are plotted: a quadratic parabola (van Soest and Bobbert 1993) and an approximation of the local relation of one sarcomere (Hatze 1977, 1981)

MTC-lengths for our isometric simulations directly from the experimental protocol. In analogy to the concentric contraction, this provides a further indication for the CE-length representing the average length of the muscle fibres. For maximum shortening in the isometric contraction mode we find $l_{m,0} - 0.85\, l_{m,0} \approx l_{CE,opt} - l_{CE}(0.85\, l_{m,0}) \approx 0.01$ m $\approx 2/3\, l_{CE,opt}$ (Fig. 8). Note that in the fully activated muscle the respective steady-state $l_{CE}(l_{m,0})$ is significantly lower than $l_{CE,opt}$ ($\approx 30\%$ shorter, Fig. 8) which is due to the stiffness of the SEE-lengthening by about 5 mm when loaded from passive force of 1.5 N to almost F_{max} at the preset MTC-length $l_{m,0}$. The MTC-length where the fully activated muscle produces maximum isometric force (i.e., $l_{CE} = l_{CE,opt}$) turns out to be $1.07 \ldots 1.08\, l_{m,0}$. For $l_m = 1.1\, l_{m,0}$ the fully activated CE ends up just slightly above (1 mm) the optimal CE-length at $l_{CE} \approx 1.07\, l_{CE,opt}$. Therefore, our analysis results in a highly asymmetric isometric force–length relation of the CE with a flat plateau [see Fig. 9 and compare (Rode et al. 2006]: the width for a CE force F_{CE} above $0.99\, F_{max}$ is $\approx 0.15\, l_{CE,opt} = 0.00225$ m.

3.1.5 Hill "parameters" A_{rel} and B_{rel}

The ratio of the Hill "parameters" A_{rel} and B_{rel} determines the maximum contraction velocity v_{max} (Eq. 7), the magnitude of A_{rel}, respectively B_{rel} fixes the curvature of the CE force–velocity hyperbola (Hill 1938). The evident slow rise in force of the fully activated model muscle during isometric contractions for MTC-lengths between $l_m = 0.88 \ldots 1.06\, l_{m,0}$ (Fig. 7) originates from the curvature resulting from concentric contraction analysis (Table 2). Quadruplicating A_{rel} and B_{rel} means reducing the curvature to values similar to those used for human jumping simulations (van Soest and Bobbert 1993). The model rise times within isometric contractions are then increased partly in accordance to physiology (Fig. 10). However, this curvature is only appropriate for MTC-lengths less than $l_m = l_{m,0}$. Hence, our muscle model does not fully map all dependencies of the Hill parameters on internal states, despite having implemented well established (van Soest and Bobbert 1993) dependencies $A_{rel}(l_{CE}, q)$ and $B_{rel}(l_{CE}, q)$. This is still valid for varied $F_{isom}(l_{CE})$ and $B_{rel}(q)$ functions. Additionally, as in quick-release and concentric contractions potential history effects are visible in the experimental curves of isometric contractions (non-steady force "plateaus"). Furthermore, the influence of the curvature of the CE force–velocity hyperbola on the isometric contraction rise times is at least as significant as the time constant of the activation dynamics τ_q. The extracted characteristics of SEE, PEE, and $F_{isom}(l_{CE})$ remain the same irrespective of the influence of the CE force–velocity relation on the internal dynamics during isometric contractions.

Introducing $B_{rel}(q)$ according to Eq. 13 instead of following (van Soest and Bobbert 1993) Eq. 11 only becomes essential in movements requiring low activation levels. Within this study such muscle states only occur transiently in the early phases of isometric contractions.

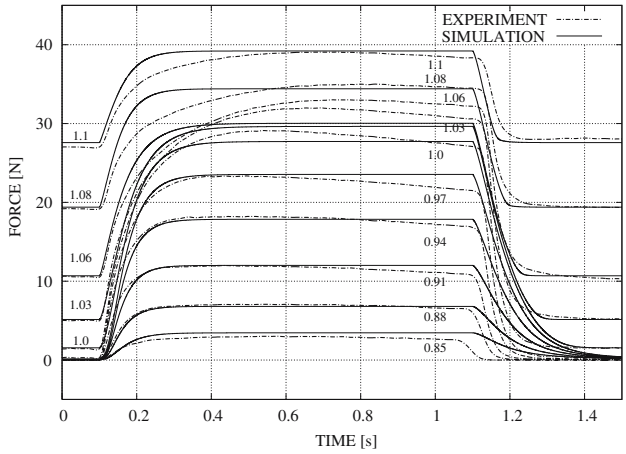

Fig. 10 Isometric contraction mode with varied Hill parameters. Force output of the MTC is plotted versus time for various fixed MTC-lengths. The experimental curves are identical to those in Fig. 7. In contrast, here all simulations were calculated with a reduced curvature (but equal $v_{\max}$) of the force–velocity relation of the model MTC. Here: $A_{\text{rel},0} = 0.4$, $B_{\text{rel},0} = 4.0\,\frac{1}{\text{s}}$ instead of $A_{\text{rel},0} = 0.1$, $B_{\text{rel},0} = 1.0\,\frac{1}{\text{s}}$ as used for all other simulations within this study (Table 2) illustrated in Figs. 5, 6, 11, 7, 8 and 12

3.2 Statements and predictions: model consequences

3.2.1 Eccentric contraction

Figures 7 and 10 reflect that an eccentric contraction is enforced after switching off the stimulation of the muscle at $t > 2\,s$. The observed fall times predicted by the model are generally too high and even increase at shorter MTC-lengths. Although not targeted in this study our muscle model yields some eccentric solution by extrapolation of the originally concentric model formulation. However, it is not surprising that this extrapolated solution barely meets physiological characteristics expecting different processes behind concentric and eccentric contraction dynamics.

3.2.2 Macroscopic versus microscopic view

The macroscopic isometric force–length relation does not only contain the single-sarcomere force–length relation but also the pennation angle ($< 20°$, $\cos 20° \approx 0.94$) within the muscle belly and the inhomogeneous distribution of a variety of muscle fibres. Introducing a macroscopic CE in the muscle model accounts for pooling these properties. The elastic components (SEE, PEE) are also macroscopic representations of microscopic properties and structures. The modelled SEE contains all passive elastic substructures as e.g., aponeurosis, fascia, tendon, and (potentially activation-dependent) titin molecules. However, the elastic characteristics are more directly derivable from the analysis of our experiments. The macroscopic isometric force–length relation (F_{isom}, Fig. 9) then arises more indirectly from the whole validation process of our complex muscle model strongly depending on the elastic characteristics. Essentially, $F_{\text{isom}}(l_{\text{CE}})$ emerges with an asymmetry contrary to the single sarcomere findings: the ascending limb is broader and less inclined than the descending limb (Sect. 3.1.4). The force–length relation of our (piglet) muscle has a plateau much broader than that predicted by other model approaches [Fig. 9; (Hatze 1977, 1981; van Soest and Bobbert 1993)].

3.2.3 Damping

Figure 11 again illustrates the 100 g case from Fig. 6 (experiment and simulation) varying damping elements in the model MTC. The simulation results with the model including the Hill-type CE force–velocity relation and additionally a force-dependent SE-damping (Fig. 6) are compared to three other cases (Fig. 3): neglecting any additional damping, constant PE-damping, and external damping in proportion to $\dot{l}_{\text{m}}$. Neglecting additional damping uncovers the eigenoscillation induced by the coupling of the SEE and the loading mass (compare Sect. 3.1.2). Adding a constant PE-damping element amplifies the oscillation. This emphasises our statement in Sect. 3.1.2 that the presence of a damping element in series to the SEE makes the connection point between CE and SEE an effective suspension for the SEE-mass system. Consequently, PE-damping simply enhances the already present damping of the Hill-type element (CE). Infinite damping

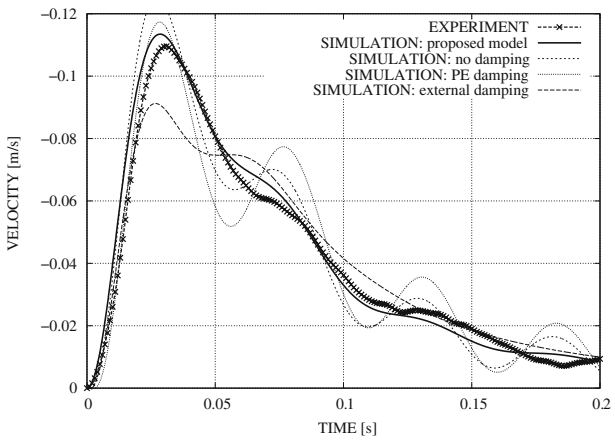

Fig. 11 Concentric contraction with varied damping elements. As an example the 100 g case from Fig. 6 is plotted again (experiment: *crossed dashed line*; simulation including force-dependent serial damping according to Sect. 2.2.6 with $d_{\text{SE,max}} = 60\,\text{Ns/m}$ and $F_{\text{CE}}/F_{\max} \approx 1/30$: *thick solid line*). Additionally, the simulation results for three further cases are presented for comparison: (i) leaving out any internal (serial or parallel) damping (*dashed line*), (ii) introducing parallel (according to Sect. 2.2.4: $d_{\text{PE}} = 6\,\text{Ns/m}$) instead of serial damping (*dotted line*), and (iii) leaving out any internal but using external damping ($d_{\text{ext}} = 6\,\text{Ns/m}$) in proportion to the MTC-velocity (*dash-dotted line*)

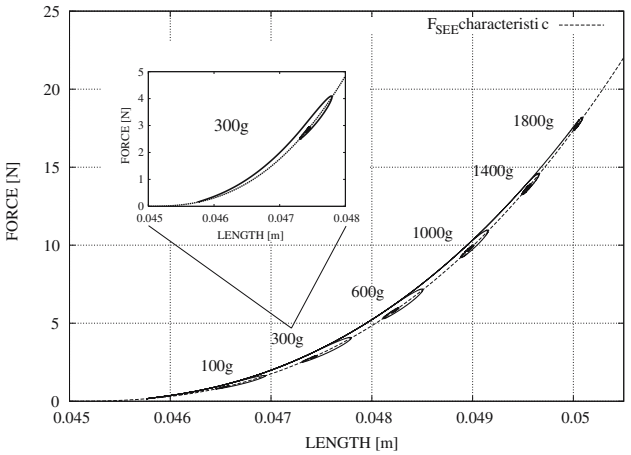

Fig. 12 Simulated (dynamic) force–length relation(s) of the SE during concentric contractions. Here, the simulation data presented in Fig. 6 are (re-)plotted using different variables: the SE-length as abscissa and the SE-force (i.e., the sum of SEE-force and SE damping force equating the MTC force output) as ordinate. Thereby, time runs as a parameter along a dynamic force–length relation of the SE (*solid lines*) each of which represents the contraction dynamics of a specific load (given in *g*). The inset shows the zoomed dynamic relation for the 300 g case. For all loads the dynamic force–length relations of the SE deviate moderately from the force–length relation of the SEE (*dashed line*). Thus, the (force-dependent) SE-damping according to Sect. 2.2.6 lies well within physiological limits (compare e.g., (Shadwick 1990)). The parameters of the SEE and the SE-damping are condensed in Table 2. The non-linear-linear transition of the SEE lies beyond the limits suitable to illustrate the concentric contraction dynamics of all simulated loads. Each dynamic force–length relation approaches via a damped eigen oscillation the point on the force–length relation of the SEE where the SEE-force is in static equilibrium with the weight of the loading mass

would be equivalent to an ideally rigid suspension showing maximum amplification. Decreased PE-damping reduces the oscillatory amplitude. However, the dissipative character of the CE is immanent to a Hill-type muscle. Thus, the only remaining strategy within the element structure of the muscle model (Fig. 3) is to introduce damping immediately into the SEE-mass system (i.e., in parallel with the SEE). Using linear SE-damping with a constant, force-independent damping coefficient being appropriate for the highest analysed load (1,800 g) leads to clear cut over-damping of the concentric contraction dynamics of the lowest load. We found that an SE-damping coefficient depending on the CE force F_{CE} is able to suppress the eigenfrequency of the SEE-mass system properly for the whole range of analysed loads (Fig. 12). Introducing external damping does not even enable one to reproduce the contraction dynamics for one single load within the first 0.2 s.

4 Discussion

This study provides two main results. First, we found that additional de-localised damping is crucial to suppress the SEE-load eigenfrequency when utilising standard Hill-type muscle models (Fig. 3) in computer simulations. Second, even when applying an SE-damped Hill-type model, it is not possible to reproduce accurately both concentric contractions and force development during isometric contractions using the same set of Hill "parameters" A_{rel} and B_{rel} within simulations. Besides, we will discuss consequences of discrepancies between the output of the experimental muscle and the Hill-type model used for representation. However, we would like to start our discussion with emphasising the significance of choosing the model MTC-length equal to the anatomical MTC-length.

4.1 The significance of $l_{m,0}$

There are at least three weighty reasons for the typical model MTC-length $l_{m,0}$ to be set closely to the mean anatomical MTC-length l_0 (within its experimental determinability). First, all experimental length conditions are directly transferable to model constraints. Second, as a result, the determined parameters e.g., of the non-linear characteristics of SEE and PEE receive an immediate physiological meaning. Third, the muscle model both preserves and obtains its potential of transparent scalability and therefore of model portability.

For the reason of optimal consistency of experiment and model $l_{SEE,0}$ was chosen as the difference between l_0 and the typical fibre length ($l_{CE,opt}$) in anatomical position (l_0). Because of the aforementioned indeterminacies there remains a small range (a few millimetres) of model MTC-lengths to fulfil $l_{m,0} \approx l_{SEE,0} + l_{CE,opt}$. The choice of $l_{m,0}$ is restricted because of the preset SEE-stiffness (from quick-release), the pretty unambiguous exponent ($\nu_{SEE,PEE} = 2.5$) of the passive compound stiffness (SEE and PEE in series) and the fixed MTC-length steps (isometric contractions). Hence, if force and therefore length of the SEE is known from experiment in the isometric condition $l_{m,0}$ selecting a longer model muscle (higher $l_{m,0}$) can only be compensated by varying the PEE-characteristics. As a consequence in the derived isometric force–length relation $F_{isom}(l_{CE})$, the part of the force plateau of the ascending limb ($l_{CE} < l_{CE,opt}$) is reduced with increasing $l_{m,0}$ in advantage of that of the descending limb. The ascending tail reaching to very short l_{CE} becomes flatter. The descending tail seems to have more theoretical significance. For, it is functionally not accessible in the intact muscle because the stiffness of the PEE is high enough to take over stress almost completely from the CE if the MTC is lengthened by less than $0.1\, l_{CE,opt}$ starting where the isometric force level has descended to $0.99\, F_{max}$ (leaving the force plateau). In this sense the asymmetry of the identified macroscopic isometric force–length relation is somehow virtual and does not contradict the force–length relation of a single sarcomere. Even though, the taking-over region from CE to PEE is well quantifiable by our experimental data.

4.2 Damping

The extremely reduced experimental situation of analysing one muscle working on one mechanical degree of freedom (loading mass) reveals the basic deficiency of standard Hill-type muscle models: the luring eigenoscillation is initiated during simulation of concentric contractions starting with an initially resting load if damping in the SE is neglected in the model. In the real muscle this oscillation is damped physiologically. This means that damping locally present merely in one part of the MTC (e.g., the Hill-type CE and/or any damping in parallel to the CE) is insufficient to suppress the oscillatory interaction between undamped parts of the MTC and the load. In this sense physiology points to de-localised (along the MTC) musculo-tendinous damping.

Apart from model validity this de-localised MTC-damping is of significance for the use of Hill-type muscle models in multi-body simulations of musculo-skeletal systems, including segmental masses ranging over an order of magnitude. A sudden release or excitation of a mechanical degree of freedom (e.g., heel lift during push off or leg impact during landing) may occur during biomechanical movement situations leading to increased numerical costs or even stiff equations (not integrable).

We found typical eigenfrequencies between 10 and 20 Hz for our piglet muscle, which lie in the vicinity of soft-tissue oscillations known from literature (Denoth 1985; Gruber et al. 1998; Wakeling and Nigg 2001; Wilson et al. 2001; Günther et al. 2003; Pain and Challis 2006). One could speculate that the typical passive elasticities within the MTC determine the frequencies of those impact induced soft-tissue oscillations just alike. Furthermore, it is known that these oscillations are damped slightly under-critically as can also be confirmed by this study.

Elasticity is a fundamental principle for efficient fast locomotion (Cavagna 1970; Alexander 1988; Blickhan 1989; McMahon and Cheng 1990). Here, vibrations classified as bad or hazardous (Wilson et al. 2001; Alexander 2001) are induced. Alexander (2001) doubts that the low damping coefficient (93% efficiency) of the tendon suffices to damp these MTC-vibrations. Therefore, he excluded the tendon to be the location for damping. Although, he acknowledged tendons e.g., of horses to heat up during races (Wilson and Goodship 1994) indicating relevant damping (Ker 1981; Riemersma and Schamhardt 1985). In contrast, according to our model calculations an SE-damping as low as given in literature (Ker 1981; Riemersma and Schamhardt 1985; Shadwick 1990; Krause et al. 1995; Alexander 2001) (see Fig. 12) does the job perfectly if SE-damping approximately equates CE-damping. The SE-damping coefficient lies in the range 1–10 Ns/m (depending on q, l_{CE} and F_{CE}). The CE-damping coefficient is the current slope of the force-velocity relation (e.g., $F_{max}\, q\, F_{isom}/v_{max} \cdot A_{rel}/(1 + A_{rel})$ at v_{max}). Also, in the study of Wilson et al. (2001) the simpler phenomenological muscle model describing the MTC-damping allows for a better reproduction of the frequency dependency of vibrational damping than the microscopic muscle fibre model (Piazzesi and Lombardi 1995, 1996)again pointing to de-localised MTC-damping.

In muscle fibres, the giant protein titin is attached at the M-line (connecting the myosin molecules in the centre of the sarcomere), tunnels through the thick filament (myosin), and further bridges the gap to the Z-line (connecting to actin molecules terminating the sarcomere). Therefore, titin can represent both serial and parallel structures to the contractile machinery (attached actin–myosin cross-bridge) represented by CE in the muscle model (Reconditi et al. 2004; Lan and Sun 2005). Thus, if there is at least one attached cross-bridge in a sarcomere all parts of actin and myosin other than the attached region get a serial meaning just like the elasticity of the cross-bridge itself (Lombardi et al. 1995; Lan and Sun 2005). In this sense, the titin section bridging the gap between myosin and the Z-line (I-band) represents a parallel visco-elastic element (Carrion-Vazquez et al. 1999; Marszalek et al. 1999; Minajeva et al. 2001; Tskhovrebova and Trinick 2002; Telley et al. 2003). Knowing the high re-folding rates of titin (up to 100 Hz) for low amplitude stretches (Carrion-Vazquez et al. 1999; Marszalek et al. 1999; Minajeva et al. 2001), one could speculate that the damping within the sarcomere is explained rather by this parallel titin visco-elasticity than by the force–velocity relation of the contractile machinery. Moreover, if e.g., the titin section tunnelling myosin (A-band) moved relative to myosin while mechanically interacting a passive serial damping would occur (Tskhovrebova and Trinick 2002; Lombardi et al. 2004).

In essence, de-localised MTC-damping can be viewed as a purely passive phenomenon both within the sarcomere and the macroscopic serial elements (tendon and aponeurosis).

4.3 The Hill relation

Our triple contraction mode analysis enabled us first to identify a consistent set of the passive visco-elastic properties of one piglet MTC. Second, based on that we could track down the curvature (not the parameter v_{max}) of the Hill relation to be the crucial parameter for fitting the contraction dynamics of the MTC under all three external constraints. In turn, this means that fitting one unique set of Hill parameters A_{rel}, B_{rel} is inadequate to accurately explain the contraction dynamics even for the three analysed conventional contraction modes.

Additionally, the manifold application of the Hill relation in literature demonstrates that one can find a physiologically valid choice of Hill muscle parameters for various contraction modes, muscle groups, internal or environmental parameters (e.g., muscle preparation or state, temperature, biochemical state), animal species and their states of development.

However, such a specific parametrisation can only be used for the simulation of a motor task in which the conditions of the experimental muscle preparation match that of the selected motor task as e.g., in jumping situations (van Soest 1992). Our muscle was analysed in modes typically occurring during jumping movements (concentric and quick-release contraction), however, its curvature is more pronounced than that of human volleyball players (van Soest 1992). This is a further indication of the dependency of the Hill parameters on the specific experimental situation hampering scalability of a Hill-type muscle model. This ambiguity of muscle parameters originates from the Hill-type model being a phenomenological model. Therefore, we agree with Epstein and Herzog (2003) that it can neither provide a causal explanation of physiological processes nor be used for an unambiguous prediction of model CE-dynamics. Consequently, in our view there is dire necessity to develop a macroscopic muscle-tendon model in which the Hill relation is not used as the local law describing the contraction dynamics of the CE which represents the contractile machinery. Therefore, the inter-relation of the passive visco-elastic properties of the MTC, the contractile machinery, the respective model element (CE), and the specific modelling of the dynamic characteristics of the CE has to be re-formulated (Denoth et al. 2002).

4.4 Evolution of macroscopic muscle models

The very low dimensional Hill-type muscle model formulated by van Soest and Bobbert (1993) still shows discrepancies to the output of the real MTC after introduction of force-dependent SE-damping. Nevertheless, just one force characteristic of the model had to be revised to eliminate non-physiological predictions of oscillations. Taking the non-linearity of the SEE into account follows the same strategy of model evolution by rewriting a force characteristic to enhance physiological validity. Here, a realistic homogenisation of the frequency response under various loads was achieved. In contrast, this strategy cannot be applied to the modelling of hysteresis effects. Rather this requires the introduction of at least one additional degree of freedom within the muscle model (Meijer et al. 1998). However, in our view there is no need for changing the strategy of using and evolving a macroscopic approach to muscle modelling and to favour multi-dimensional, multi-parametric microscopic models instead. Beyond a numerical efficiency superior to microscopic models, a reduced macroscopic model plays one of three crucial roles in understanding the fundamental principles underlying dynamic processes. Measurements of real world phenomena play the first role. Predictions of microscopic models play the second role. But how can we understand the self-organisation of those millions of sarcomeres if not by explicitly formulating their macroscopic effect?

Acknowledgments MG was supported by the grants MU1766/1-1, MU1766/1-2, and BL236/11-1 of the "Deutsche Forschungsgemeinschaft" (DFG). VW would like to thank PD Dr. Reinhard Bauer (Institute of Molecular Cell Biology, Pathophysiology Lab, Friedrich–Schiller–Universität, Jena, Germany) for support and assistance during the muscle experiments. MG and SS thank Anton Prochel for useful checks to verify the numerical integration of the muscle model.

References

Alexander RMcN (1988) Elastic mechanisms in animal movement. Cambrigde University Press, Cambridge

Alexander RMcN (2001) Damper for bad vibrations. Nature 414(6866):855–857

Biewener AA (1990) Biomechanics of mammalian terrestrial locomotion. Science 250(4984):1097–1103

Blickhan R (1989) The spring-mass model for running and hopping. J Biomech 22(11/12):1217–1227

Carrion-Vazquez M, Oberhauser AF, Fowler SB, Marszalek PE, Broedel SE, Clarke J, Fernandez JM (1999) Mechanical and chemical unfolding of a single protein: a comparison. Proc Natl Acad Sci USA 96(7):3694–3699

Cavagna GA (1970) Elastic bounce of the body. J Appl Physiol 29(3):279–282

Chow JW, Darling WG (1999) The maximum shortening velocity of muscle should be scaled with activation. J Appl Physiol 86(3):1025–1031

Currey JD (2002) Bones: structure and mechanics. Princeton University Press, Princeton, NJ

Davy DT, Audu ML (1987) A dynamic optimization technique for predicting muscle forces in the swing phase of gait. J Biomech 20(2):187–201

Denoth J (1985) The dynamic behaviour of a three link model of the human body during impact with the ground. In: Winter DA, Norman RW, Wells RP, Hayes KC, Patla AE (eds), Biomechanics 9-A, vol 5B of International Series on Biomechanics. Human Kinetics Publishers, Champaign, pp 102–106

Denoth J, Stüssi E, Csucs G, Danuser G (2002) Single muscle fiber contraction is dictated by inter-sarcomere dynamics. J Theor Biol 216(1):101–122

Epstein M, Herzog W (2003) Aspects of skeletal muscle modelling. Philos Trans R Soc Lond B 358(1437):1445–1452

Ettema GJ, Meijer K (2000) Muscle contraction history: modified Hill versus an exponential decay model. Biol Cybern 83(6):491–500

Gordon AM, Huxley AF, Julian FJ (1966) The variation in isometric tension with sarcomere length in vertebrate muscle fibers. J Physiol 184:170–192

Granzier HL, Labeit S (2006) The giant muscle protein titin is an adjustable molecular spring. Exerc Sport Sci Rev 34(2):50–53

Gruber K, Ruder H, Denoth J, Schneider K (1998) A comparative study of impact dynamics: wobbling mass model versus rigid body models. J Biomech 31(5):439–444

Günther M, Ruder H (2003) Synthesis of two-dimensional human walking: a test of the λ-model. Biol Cybern 89(2):89–106

Günther M, Sholukha VA, Keßler D, Wank V, Blickhan R (2003) Dealing with skin motion and wobbling masses in inverse dynamics. J Mech Med Biol 3(3/4):309–335

Hatze H (1977) A myocybernetic control model of skeletal muscle. Biol Cybern 25:103–119

Hatze H (1981) Myocybernetic control models of skeletal muscle — characteristics and applications. University of South Africa Press, Pretoria

Hill AV (1938) The heat of shortening and the dynamic constants of muscle. Proc R Soc Lond B 126:136–195

Julian FJ (1971) The effect of calcium on the force-velocity relation of briefly glycerinated frog muscle fibres. J Physiol 218:117–145
Katz B (1939) The relation between force and speed in muscular contraction. J Physiol 96:45–64
Ker RF (1981) Dynamic tensile properties of the plantaris tendon of sheep (Ovis aries). J Exp Biol 93:283–302
Ker RF, Wang XT, Pike AV (2000) Fatigue quality of mammalian tendons. J Exp Biol 203(Pt 8):1317–1327
Ker RF, Zioupos P (1997) Creep and fatigue damage of mammalian tendon and bone. Comments Theor Biol 4(2-3):151–181
Kistemaker DA, van Soest AJ, Bobbert MF (2006) Is equilibrium point control feasible for fast goal-directed single-joint movements? J Neurophysiol 95(5):2898–2912
Krause PC, Choi JS, McMahon TA (1995) The force-velocity curve in passive whole muscle is asymmetric about zero velocity. J Biomech 28(9):1035–1043
Krieg M (1992) Simulation und Steuerung biomechanischer Mehrkörpersysteme. Master's thesis. Eberhard-Karls-Universität, Tübingen, Germany
Lan G, Sun SX (2005) Dynamics of myosin-driven skeletal muscle contraction: I. Steady-state force generation. Biophys J 88(6):4107–4117
Lombardi V, Piazzesi G, Ferenczi MA, Thirlwell H, Dobbie I, Irving M (1995) Elastic distortion of myosin heads and repriming of the working stroke in muscle. Nature 374(6522):553–555
Lombardi V, Piazzesi G, Reconditi M, Linari M, Lucii L, Stewart A, Sun YB, Boesecke P, Narayanan T, Irving T, Irving M (2004) X-ray diffraction studies of the contractile mechanism in single muscle fibres. Philos Trans R Soc Lond B 359(1452):1883–1893
Marszalek PE, Lu H, Li H, Carrion-Vazquez M, Oberhauser AF, Schulten K, Fernandez JM (1999) Mechanical unfolding intermediates in titin modules. Nature 402(6757):100–103
McMahon TA, Cheng GC (1990) The mechanics of running: how does stiffness couple with speed? J Biomech 23(Suppl. 1):65–78
Meijer K, Grootenboer HJ, Koopman HF, van der Linden BJ, Huijing PA (1998) A Hill type model of rat medial gastrocnemius muscle that accounts for shortening history effects. J Biomech 31(6):555–563
Minajeva A, Kulke M, Fernandez JM, Linke WA (2001) Unfolding of titin domains explains the viscoelastic behavior of skeletal myofibrils. Biophys J 80(3):1442–1451
Pain MTG, Challis JH (2006) The influence of soft tissue movement on ground reaction forces, joint torques and reaction forces in drop landings. J Biomech 39(1):119–124
Petrofsky JS, Phillips CA (1981) The influence of temperature, initial length and electrical activity on force-velocity relationship of the medial gastrocnemius muscle of the cat. J Biomech 14(5):297–306
Piazzesi G, Lombardi V (1995) A cross-bridge model that is able to explain mechanical and energetic properties of shortening muscle. Biophys J 68(5):1966–1979
Piazzesi G, Lombardi V (1996) Simulation of the rapid regeneration of the actin-myosin working stroke with a tight coupling model of muscle contraction. J Muscle Res Cell Motil 17(1):45–53
Press WH, Teukolsky SA, Vetterling WT, Flannery BP (1994) Numerical recipes in C—the art of scientific computing, 2nd edn. Cambridge University Press, Cambridge
Proske U, Morgan DL (1987) Tendon stiffness: methods of measurement and significance for the control of movement. A review. J Biomech 20(1):75–82
Reconditi M, Linari M, Lucii L, Stewart A, Sun YB, Boesecke P, Narayanan T, Fischetti RF, Irving T, Piazzesi G, Irving M, Lombardi V (2004) The myosin motor in muscle generates a smaller and slower working stroke at higher load. Nature 428(6982):578–581
Reinsch CH (1967) Smoothing by spline functions. Numerische Mathematik 10(3):177–183
Riemersma DJ, Schamhardt HC (1985) In vitro mechanical properties of equine tendons in relation to cross-sectional area and collagen content. Res Vet Sci 39(3):263–270
Rode C, Siebert T, Herzog W, Blickhan R (2006) The effects of parallel and series elastic components on estimated active muscle force (submitted to the J Biomech)
Schmalz T (1993a) Biomechanische Modellierung menschlicher Bewegung, vol 26 of Wissenschaftliche Schriftenreihe des Deutschen Sportbundes. Karl Hofmann, Schorndorf, Germany
Schmalz T (1993b) Die Nutzung biomechanischer Modelle zur Bestimmung rheologischer Eigenschaften des Muskel-Sehnen-Komplexes. In: Gutewort W, Schmalz T, Weiß T (eds), Symposium Oberhof: Aktuelle Hauptforschungsrichtungen der Biomechanik sportlicher Bewegungen, vol 55, Sankt Augustin, Germany, 1993. Deutsche Vereinigung für Sportwissenschaft (dvs), Academia, pp 102–108
Shadwick RE (1990) Elastic energy storage in tendons: mechanical differences related to function and age. J Appl Physiol 68(3):1033–1040
Shampine LF, Gordon MK (1975) Computer solution of ordinary differential equations: the initial value problem. W.H. Freeman & Co., San Francisco
Siebert T, Wagner H, Blickhan R (2003) Not all oscillations are rubbish: forward simulation of quick-release experiments. J Mech Med Biol 3(1):107–122
Stern JT (1974) Computer modeling of gross muscle dynamics. J Biomech 7:411–428
Telley IA, Denoth J, Ranatunga KW (2003) Inter-sarcomere dynamics in muscle fibres. A neglected subject? Adv Exp Med Biol 538:481–500
Tskhovrebova L, Trinick J (2002) Role of titin in vertebrate striated muscle. Philos Trans R Soc Lond B 357(1418):199–206
van Ingen Schenau GJ (1984) An alternative view to the concept of utilization of elastic energy. Hum Mov Sci 3:301–336
van Leeuwen JL (1992) Muscle function in locomotion. In: Alexander RMcN (ed) Advances in comparative and environmental physiology, vol 11, chap 7. Springer, Berlin, pp 191–250
van Soest AJ (1992) Jumping from structure to control: a simulation study of explosive movements. PhD thesis, Vrije Universiteit, Amsterdam
van Soest AJ, Bobbert MF (1993) The contribution of muscle properties in the control of explosive movements. Biol Cybern 69(3):195–204
Wakeling JM, Nigg BM (2001) Soft-tissue vibrations in the quadriceps measured with skin mounted transducers. J Biomech 34(4):539–543
Wank V (2000) Aufbau und Anwendung von Muskel-Skelett-Modellen. Habilitationsschrift der Friedrich-Schiller-Universität Jena
Wank V, Bauer R, Walter B, Kluge H, Fischer MS, Blickhan R, Zwiener U (2000) Accelerated contractile function and improved fatigue resistance of calf muscles in newborn piglets with IUGR. Am J Physiol Regul Integr Comp Physiol 278(2):R304–R310
Wank V, Fischer MS, Walter B, Bauer R (2006) Muscle growth and fiber type composition in hind limb muscles during postnatal development in pigs. Cells Tissues Organs 182(3-4):171–181
Wilson AM, Goodship AE (1994) Exercise-induced hyperthermia as a possible mechanism for tendon degeneration. J Biomech 27(7):899–905
Wilson AM, McGuigan MP, Su A, van den Bogert AJ (2001) Horses damp the spring in their step. Nature 414(6866):895–899
Zajac FE (1989) Muscle and tendon: properties, models, scaling, and application to biomechanics and motor control. In: Bourne JR (ed) CRC critical reviews in biomedical engineering, vol 17. CRC Press, Boca Raton, pp 359–411
Zioupos P, Currey JD, Casinos A (2001) Tensile fatigue in bone: are cycles-, or time to failure, or both, important? J Theor Biol 210(3):389–399